POLITECNICO DI TORINO
Repository ISTITUZIONALE

A Spirulina-derived pigment extract combining phycocyanin and chlorophyll for optically responsive photopolymer architectures

Original
A Spirulina-derived pigment extract combining phycocyanin and chlorophyll for optically responsive photopolymer architectures / Olla, C., Martis, A., Barontini, C., Carbonaro, C.M., Roppolo, I., Ricci, P.C., Secci, F., Chiappone, A.. - In: SUSTAINABLE MATERIALS AND TECHNOLOGIES. - ISSN 2214-9937. - 49:(2026), pp. 1-16. [10.1016/j.susmat.2026.e02096]

Availability:
This version is available at: 11583/3017465 since: 2026-11-03T12:12:00Z

Publisher:
Elsevier

Published
DOI:10.1016/j.susmat.2026.e02096

Terms of use:

This article is made available under terms and conditions as specified in the corresponding bibliographic description in the repository

Publisher copyright

(Article begins on next page)

21 November 2026

Sustainable Materials and Technologies 49 (2026) e02096

Contents lists available at ScienceDirect

Sustainable Materials and Technologies

journal homepage: www.elsevier.com/locate/susmat

A Spirulina-derived pigment extract combining phycocyanin and chlorophyll for optically responsive photopolymer architectures

Chiara Olla [a,*], Alberto Martis [b], Carlo Barontini [c], Carlo Maria Carbonaro [a], Ignazio Roppolo [b,d], Pier Carlo Ricci [a], Francesco Secci [c], Annalisa Chiappone [c,*]

[a] Department of Physics, University of Cagliari, Cittadella Universitaria, Monserrato, 09042, Italy
[b] Center for Sustainable Future Technologies (CSFT)@Polito, Istituto Italiano di Tecnologia, Via Livorno 60, Turin, 10144, Italy
[c] Department of Chemical and Geological Sciences, University of Cagliari, Cittadella Universitaria, Monserrato, 09042, Italy
[d] Department of Applied Science and Technology, Politecnico di Torino, Corso Duca degli Abruzzi 24, Turin, 10129, Italy

ARTICLE INFO

Keywords:
Spirulina
Phycocyanin
Bio-derived additives
DLP 3D printing
Optical sensing

ABSTRACT

The optical response of a Spirulina-derived extract (SP-E), containing phycocyanin and chlorophyll-derived pigments, was investigated in liquid and solid-state environments, deliberately exploiting extract complexity rather than pigment purification to develop a sustainable optical platform. In aqueous media, SP-E displayed the characteristic signatures of phycocyanin, whereas exposure to organic solvents, basic conditions, or oxidative agents induced pronounced blue-to-green/yellow transitions driven by attenuation of the phycocyanin contribution and enhanced visibility of chlorophyll-derived species. When incorporated into PEGDA700 photopolymers, SP-E retained chemically responsive colorimetric behavior toward both liquid and vapor/headspace chemical environments. For aqueous ammonia, a quantitative proof-of-concept response was obtained using a ratiometric signal, yielding a limit of detection of 0.41% v/v NH_3, and an apparent response time of approximately 10 min. The optical response was strongly influenced by photopolymerization conditions, as high photoinitiator/SP-E ratios promoted attenuation of the phycocyanin-related signature; this behavior was supported by independent oxidation and photoinitiator-assisted irradiation experiments. Integration of SP-E into digital light processing formulations enabled fabrication of optically active 3D architectures with luminescence-based chemical indication, while the intrinsic light-attenuating properties of the multi-pigment extract contributed to printing control. Altogether, SP-E emerges as a multifunctional, sustainable additive that combines environmental optical responsiveness with photopolymer processability and compatibility with additive manufacturing, offering a resource-efficient route toward bio-derived optical indicators and functional printed materials.

1. Introduction

Phycobiliproteins are highly conjugated pigment–protein complexes responsible for the characteristic blue and red coloration of cyanobacteria and red algae. Among them, C-phycocyanin (PCN) is the major water-soluble chromoprotein of Spirulina, the common name of *Arthrospira platensis*, where it functions as a light-harvesting antenna within the photosynthetic apparatus [1–3]. Its intense blue coloration and bright red fluorescence arise from covalently bound phycocyanobilin (PCB) chromophores, whose optical behavior is strongly modulated by the surrounding protein environment [4–7]. In its free molecular form, obtained through different isolation procedures [8–10], PCB exhibits solvent-dependent conformational switching and proton-transfer dynamics [11–13], whereas in the native protein scaffold the local environment governs chromophore accessibility, stabilization, and quenching pathways [14].

Beyond their biological relevance, PCN and related biliproteins possess well-documented anticancer, anti inflammatory, and antioxidant properties, which have led to their use in pharmaceutical and nutraceutical formulations [15–18]. At the same time, their intense visible absorption, high fluorescence quantum yield, and sensitivity to the chemical environment make them attractive for photonic, sensing, and bio-optoelectronic applications [19–23]. Colorimetric and luminescent strategies based on environmentally responsive bio-derived and organic emitters have been widely explored for chemical sensing, including ratiometric approaches that enhance signal robustness and reliability [24–27]. In addition, bilin chromophores display remarkable

* Corresponding authors.
E-mail addresses: chiara.olla@dsf.unica.it (C. Olla), annalisa.chiappone@unica.it (A. Chiappone).
[1] Created in BioRender. C. (2026) https://BioRender.com/563yy7a

https://doi.org/10.1016/j.susmat.2026.e02096
Received 6 March 2026; Received in revised form 26 May 2026; Accepted 27 May 2026
Available online 8 June 2026
2214-9937/© 2026 The Authors. Published by Elsevier B.V. This is an open access article under the CC BY license (http://creativecommons.org/licenses/by/4.0/).

reactivity toward radical species, acting as efficient scavengers and optical reporters of oxidative environments [28–31]. This potential coupling between optical and environmental responsiveness makes phycobiliproteins appealing building blocks for chemically responsive materials and colorimetric/luminescent indicator systems.

At the applied level, Spirulina represents a practical and sustainable pigment source, being one of the most extensively studied cyanobacteria. Its large-scale cultivation is cost-effective, environmentally resilient, and readily integrated into food, cosmetic, and biomedical production chains [2,20,32]. However, Spirulina-derived extracts are inherently complex mixtures that, besides PCN, mainly include chlorophyll-derived species and accessory pigments with distinct optical responses, which are often removed in conventional purification strategies aimed at isolating the blue fraction [33,34].

Rather than representing a limitation, this compositional complexity offers access to a broad palette of optical behaviors that can be modulated by solvent polarity, pH, and redox conditions. Understanding how different chromophoric fractions respond to environmental stimuli, both when isolated and when coexisting within the same extract, is therefore essential to assess their potential as colorimetric or luminescent probes. In this perspective, a zero-waste approach enables the valorization of multiple pigment components present in the extract, avoiding unnecessary purification steps and allowing non-blue fractions to be exploited for technological applications [35–37].

Among chemically relevant stimuli, interactions with ammonia and formaldehyde are of particular interest. Beyond their fundamental impact on protein conformation and pigment binding, these compounds are widely recognized as toxic volatile pollutants, whose detection is important for environmental monitoring and occupational safety [38,39]. The sensitivity of phycobiliprotein-based systems to such analytes makes Spirulina-derived pigments promising candidates for sustainable optical indication and sensing strategies.

Embedding biochromophoric systems into polymeric matrices provides a viable route to enhance their stability and translate solution-phase optical responsiveness into solid-state materials. Poly(ethylene glycol) diacrylate (PEGDA) networks obtained by photopolymerization combine high optical transparency, adjustable permeability, and chemical compatibility with water-soluble biomolecules. Moreover, their compatibility with digital light processing (DLP) 3D printing enables the fabrication of customizable optical elements and architectures with micrometer-scale features [40–44]. In this context, the incorporation of colored or fluorescent additives into photocurable resins plays a dual role, as spectral overlap and radical interactions between the photoinitiator and the chromophore can critically influence both curing efficiency and print definition. At the same time, such chromophores can endow the resulting printed architectures with intrinsic optical functionality, potentially enabling the direct fabrication of optically responsive 3D devices.

Several studies have addressed the biochemical properties of purified phycocyanin or pigment production under different illumination conditions [6,23,45,46]. However, comprehensive photophysical analyses of complex Spirulina-derived extracts remain limited, especially in the solid state and in their native multi-pigment composition. Most available works investigating optical properties focus either on isolated chromophores or on photostability for nutraceutical purposes, leaving the collective optical response of mixed pigment systems, particularly under solid-state and photopolymerization conditions, largely unexplored [3,8,9,11,47].

In this work, we investigate the optical behavior of a blue–green Spirulina-derived extract (SP-E) containing phycocyanin and chlorophyll-derived pigment families, deliberately preserving its intrinsic compositional complexity. The response of SP-E is examined in liquid media and in photopolymerized PEGDA matrices exposed to different liquid and vapor/headspace chemical environments. Through a combination of UV–Vis absorption, steady-state fluorescence, time-resolved spectroscopy, photorheological analysis, and DLP printing experiments, we elucidate the chemically induced optical responses of SP-E in aqueous ammonia, formaldehyde, methanol, and hydrogen peroxide, and evaluate its behavior when integrated into solid polymeric films and printed architectures. Overall, this study demonstrates that Spirulina-derived extracts can act as multifunctional, bio-derived additives that combine environmental and redox responsiveness with optical modulation of photopolymerization processes, offering a sustainable route toward colorimetric/luminescent optical indicators and optically functional materials compatible with additive manufacturing.

2. Experimental section

2.1. Materials

Arthrospira platensis biomass (Spirulina) was kindly provided by Livegreen Società Agricola Srl (Italy). Phycocyanin (PCN, LINABLUE® G1) was purchased from Tokyo Chemical Industry Co., and chlorophyll *a* standard was purchased from Sigma–Aldrich. Poly(ethylene glycol) diacrylate with an average molecular weight of 700 g mol^{-1} (PEGDA700, P700) was purchased from Merck. The hydroxy-functional derivative of phenylbis(2,4,6-trimethylb enzoyl)phosphine oxide (BAPO-OH) was kindly provided by Prof. Hansjörg Grützmacher (ETH, Zurich) and used as photoinitiator as received. Lithium phenyl-2,4,6-trimethylbenzoylphosphinate (LAP) was purchased from Sigma–Aldrich. Brilliant Green Dye was purchased from Merck and used as a conventional synthetic absorber benchmark. Methanol, formaldehyde aqueous solution, ammonia aqueous solution, chloroform and hydrogen peroxide were purchased from Sigma–Aldrich and used without further purification. All other solvents and reagents were of analytical grade. Distilled water was used in all preparations.

2.2. Preparation of the Spirulina-derived extract

Arthrospira platensis biomass was subjected to mild processing steps aimed at removing cellular debris while preserving the native pigment–protein complexes. Lyophilized and pulverized biomass was suspended in chilled distilled water at a concentration of 0.001 g mL^{-1} and stirred overnight at low temperature to promote pigment solubilization. The suspension was then centrifuged at 4200 rpm for 10 min to remove insoluble cellular debris. The resulting blue–green supernatant was collected and freeze-dried for 24 h, yielding the Spirulina-derived extract (SP-E) used throughout this work. For optical characterization, a fraction of the dried SP-E was redispersed in water and subjected to five cycles of sonication and centrifugation at 4200 rpm for 20 min. This procedure led to the separation of a blue water-soluble fraction and a green hydrophobic precipitate. These two fractions were collected and, when required, freeze-dried prior to spectroscopic analysis.

2.3. Photocurable formulation preparation and photopolymerization

Two main series of photocurable formulations were prepared based on PEGDA700 and SP-E. In the first series, the SP-E concentration was varied at 1, 5, and 10 phr, where phr denotes parts per hundred parts of resin by weight, while maintaining a constant BAPO-OH content of 0.5 phr. In the second series, the SP-E concentration was fixed at 1 phr and the photoinitiator content was varied at 0.1, 0.5, and 1 phr. Each formulation contained 50 phr of distilled water to facilitate pigment dispersion and obtain homogeneous mixtures. The components were premixed and sonicated in an ultrasonic bath for 15 min at room temperature until complete dissolution of the photoinitiator and uniform dispersion of SP-E. Unless otherwise specified, polymer disks employed for solvent and vapor exposure contained 1 phr of SP-E and 0.1 phr of BAPO-OH. Photopolymerization was carried out using a 405 nm UV-LED source under identical irradiation conditions for all samples. Liquid formulations were drop-cast into the photorheometer sample holder and irradiated for approximately 3 min at an intensity of 30 mW cm^{-2}.

The resulting polymer disks, with a diameter of approximately 2 cm and thickness of approximately 0.2 mm, were rinsed with distilled water and dried at room temperature prior to characterization. Control PEGDA films containing purified PCN were prepared using the same photopolymerization protocol, with 1 phr PCN and 0.1 phr BAPO-OH. Brilliant-green-containing PEGDA formulations were prepared as synthetic absorber benchmarks only for DLP printing experiments and were printed using the Asiga system under conditions comparable to those used for SP-E-containing test patterns. Photorheological analyses were performed to monitor curing kinetics and evaluate the influence of SP-E and photoinitiator concentrations on the polymerization behavior. Measurements were carried out at room temperature using an Anton Paar MCR 302 rheometer equipped with a parallel-plate geometry of 25 mm diameter and an in situ UV irradiation module at 405 nm. Formulations were placed between the plates with a gap of 0.3 mm and exposed to continuous irradiation at a uniform light intensity of 30 mW cm^{-2}.

2.4. Swelling, leaching, and optical-retention measurements

Water-immersion stability of SP-E-PEGDA films was evaluated by gravimetric swelling, mass-loss, leaching, and optical-retention measurements. Film samples were weighed before immersion to obtain the initial dry mass, m_{pre}, immersed in water for 30 min, gently blotted to remove excess surface water, and weighed again to obtain the swollen mass, m_{post}. The samples were then dried and reweighed to obtain the final dry mass, m_{dry}. The swelling ratio was calculated as:

$$\text{Swelling}(\%) = \frac{m_{post} - m_{pre}}{m_{pre}} \times 100.$$

Mass loss was estimated from the difference between m_{pre} and m_{dry}.

Possible release of SP-E into the surrounding aqueous medium was evaluated by monitoring the absorbance of the immersion medium at 620 nm. A calibration curve was obtained by measuring the absorbance at 620 nm of aqueous SP-E solutions at known concentrations. The absorbance of the immersion medium was then converted into an equivalent released SP-E concentration using the calibration curve. When the measured absorbance was comparable to the blank/calibration intercept, the released concentration was considered below the quantification limit of the UV–vis method.

Optical retention of the phycocyanin-related signal within the films was estimated from the reflectance-derived apparent absorbance at 620 nm before and after immersion. The reflectance-derived apparent absorbance was calculated as:

$$A_{\lambda,app} = -\log_{10}(R_\lambda/100),$$

where R_λ is the diffuse reflectance at wavelength λ expressed as a percentage. Because the films are thin and partially transparent, the $-\log R$ transformation provided absorption-like spectra consistent with the solution-phase optical signatures. However, the resulting $A_{\lambda,app}$ values were used only as reflectance-derived apparent absorbance values and not as absolute molecular absorbance. The optical retention percentage was calculated as:

$$\text{Optical retention}(\%) = \frac{A_{620,app}^{after}}{A_{620,app}^{before}} \times 100.$$

2.5. Liquid and vapor/headspace exposure tests

For liquid immersion experiments, SP-E-PEGDA films were immersed for 30 min in distilled water, 98% methanol, 15% aqueous formaldehyde, or 10% aqueous ammonia. After exposure, the films were removed from the liquid medium, gently blotted to remove excess surface liquid, and analyzed by reflectance spectroscopy. For vapor/headspace exposure tests, polymer disks were placed in open glass vials inside sealed vessels containing methanol, aqueous formaldehyde, or aqueous ammonia. The films were not in direct contact with the liquid media. Samples were kept at room temperature for 24 h and then analyzed by reflectance spectroscopy. The resulting spectra were compared with those obtained after direct liquid immersion.

PCN-containing control films were exposed to the same liquid media used for SP-E-PEGDA films, namely water, methanol, aqueous formaldehyde, and aqueous ammonia, and analyzed by reflectance spectroscopy before and after exposure.

For quantitative measurements, SP-E-PEGDA films were exposed to aqueous NH_3 solutions in the 0%–10% v/v range for 30 min. The low-concentration range, 0%–1% v/v NH_3, was used to construct the calibration curve. After exposure, the optical response of the films was evaluated from the reflectance-derived apparent absorbance values at 620 and 665 nm, calculated from the corresponding diffuse-reflectance spectra as described above.

The normalized ratiometric signal was calculated as:

$$S = \frac{(A_{665,app}/A_{620,app})_{30} - (A_{665,app}/A_{620,app})_0}{(A_{665,app}/A_{620,app})_0},$$

where the subscripts 0 and 30 indicate the pristine film and the film after 30 min exposure, respectively.

The sensitivity was defined as the slope of the linear fit in the low-concentration range. The limit of detection (LOD) was calculated according to the $3\sigma/m$ criterion, where σ is the standard deviation of the blank response, defined as the response measured for films exposed to 0% v/v NH_3 (distilled water), and m is the slope of the calibration curve [48]. Measurements were performed in triplicate and reported as mean ± standard deviation. The response time was evaluated by monitoring the time-dependent normalized ratiometric signal, $S(t)$, upon exposure to 10% v/v NH_3(aq). The resulting sigmoidal response was fitted with a Boltzmann function as an empirical descriptor of the transition, and the apparent response time was defined as the time required to reach 90% of the total signal variation.

2.6. Vat photopolymerization and DLP printing

Projection-based 3D printing experiments were conducted using two vat-photopolymerization systems to investigate both printability and representative high-resolution fabrication of SP-E-based formulations. Initial optimization of printing parameters was performed using an Anycubic Photon Mono SE MSLA printer equipped with a 405 nm LED light source, with an irradiance of approximately 30 mW cm^{-2}. The printer featured a nominal XY resolution of 51×51 μm^2, and the layer thickness was fixed at 50 μm. Resin formulations containing 5 phr SP-E and 0.5 phr BAPO-OH were employed. Exposure time per layer, bottom exposure time, and number of bottom layers were optimized experimentally. Unless otherwise specified, the optimized parameters were 4 s normal exposure time, 6 s bottom exposure time, and 8 bottom layers. Printed samples were rinsed with distilled water and dried at ambient conditions prior to characterization. Additional printing experiments were performed using an Asiga MAX UVX27 DLP printer, operating at a wavelength of 385 nm and providing a nominal XY pixel resolution of 27 μm. The layer thickness was varied between 50 and 100 μm depending on the Computer-Aided Design (CAD) geometry. To improve surface optical quality, the build platform was coated with a glass layer. After printing, samples were post-cured for 3 min in a UV chamber equipped with a medium-pressure mercury lamp with an irradiance of 12 mW cm^{-2}.

Cure-depth measurements were performed on SP-E-containing PEGDA/P700 formulations to evaluate the light-attenuating effect of the extract during photopolymerization. Resin samples were irradiated at different exposure times using light intensities of 5.9, 11.8, and 22.7 mW cm^{-2}. After irradiation, uncured resin was removed, and the thickness of the cured layer was measured using a digital caliper. The cured thickness was plotted as a function of exposure time for each

irradiance condition. Thickness values are reported with an estimated uncertainty of approximately ±0.1 mm.

To benchmark the printing behavior of SP-E-containing formulations against a conventional synthetic absorber, brilliant-green-containing formulations were prepared and printed using the Asiga MAX UVX27 DLP system under conditions comparable to those used for SP-E-containing test patterns. Printed resolution patterns containing both raised circular features and recessed holes with nominal diameters of 0.15, 0.20, 0.30, and 0.40 mm were analyzed by optical microscopy. Feature diameters were measured from microscopy images and reported as mean ± standard deviation.

The absolute dimensional deviation was calculated as:

$$|\Delta d| = |d_{\text{measured}} - d_{\text{CAD}}|.$$

To describe geometry-dependent deviations in feature size, the lateral bias was calculated as:

$$\text{LB}_{\text{raised}} = \frac{d_{\text{measured}} - d_{\text{CAD}}}{2}$$

for raised circular features, and as:

$$\text{LB}_{\text{hole}} = \frac{d_{\text{CAD}} - d_{\text{measured}}}{2}$$

for recessed holes. With this convention, positive lateral bias indicates broadening for raised features and narrowing or partial closure for recessed holes. Negative values indicate narrowing or underfilling for raised features and apparent enlargement for recessed holes.

Dimensional agreement between selected printed objects and the corresponding CAD models was assessed using a 3D optical scanner (E3, 3Shape). Acquired scans were aligned with the CAD models, and geometrical deviations were visualized as false-color three-dimensional maps. Regions with deviations below 100 μm were used to assess representative dimensional agreement for the selected printed architecture.

2.7. Optical and spectroscopic characterization

UV–vis–NIR absorption and reflectance spectra were recorded using a JASCO V-750 spectrophotometer in the 250–800 nm and 400–800 nm ranges, respectively, with a spectral bandwidth of 2 nm. Baseline corrections were performed using appropriate references, including a white Teflon reference for reflectance measurements and solvent-filled quartz cuvettes for solution measurements. Colorimetric and reflectance analyses of polymer disks were carried out using a UV–vis integrating sphere accessory in diffuse reflectance mode.

Steady-state and three-dimensional photoluminescence (PL) spectra were collected using a JASCO FP-8550 spectrofluorometer equipped with a 450 W xenon lamp. Excitation–emission maps (EEMs) were acquired in the excitation range 300–680 nm and emission range 400–800 nm, using a 5 nm bandwidth for both excitation and emission. Quantum yield measurements in solution were performed using an integrating sphere at excitation wavelengths of 620 and 665 nm.

Time-resolved photoluminescence (TR-PL) measurements were performed using 200 fs pulses generated by an optical parametric amplifier (Light Conversion TOPAS-C) pumped by a regenerative Ti:Sapphire amplifier (Coherent Libra-HE). The repetition rate was 1 kHz, and PL signals were detected using a streak camera (Hamamatsu C10910) coupled to a grating spectrometer (Princeton Instruments Acton SP-2300). Samples were measured in 1 cm path-length quartz cuvettes. The overall temporal resolution of the system was approximately 20 ps.

Transient absorption (TA) measurements were carried out using a pump–probe setup (Ultrafast Systems HELIOS-80000-UV–Vis-NIR) under ambient conditions. Excitation pulses of 200 fs at 1 kHz were generated at 800 nm and converted to the desired wavelength range using an optical parametric amplifier. White-light probe pulses were produced using a sapphire plate. Pump and probe beams were spatially overlapped in a 1 mm quartz cuvette containing SP-E dispersions with an optical density below 0.5. No pump-intensity-dependent dynamics were observed in the excitation fluence range 0.1–0.6 mJ cm^{-2}.

^{1}H NMR spectra were recorded on a Bruker Avance III HD 600 spectrometer (14.09 T, ^{1}H frequency 600 MHz). The water-soluble SP-E fraction and a phycocyanin-related reference compound were analyzed in D_2O, whereas the hydrophobic SP-E fraction and chlorophyll *a* reference were analyzed in $CDCl_3$.

ATR-FTIR spectra were recorded using a JASCO FT/IR-4X spectrometer equipped with an ATR accessory. Spectra were acquired in the 4000–400 cm^{-1} range with a resolution of 0.5 cm^{-1}. The relative conversion after curing was estimated from the decrease of the characteristic C=C band (1635 cm^{-1}), normalized to the carbonyl band of PEGDA selected as an internal reference (C=O, 1720 cm^{-1}). The relative conversion was calculated as:

$$\text{Conversion}(\%) = \left[1 - \frac{(T_{\text{C=C}}/T_{\text{ref}})_{\text{cured}}}{(T_{\text{C=C}}/T_{\text{ref}})_{\text{uncured}}}\right] \times 100.$$

The resulting values are reported as relative conversion because the measurements were performed on irradiated samples rather than acquired as continuous real-time FTIR kinetic traces.

Optical microscopy images of bulk-photopolymerized films and DLP-printed samples were acquired under visible light and UV excitation using a Nikon Eclipse Ni microscope (Nikon Instruments Europe BV, Amsterdam, The Netherlands).

3. Results and discussion

3.1. Standard optical properties

The optical properties of the Spirulina-derived extract (SP-E) were first investigated to identify the spectral signatures of its main chromophoric components. Steady-state diffuse reflectance and photoluminescence measurements were carried out on the whole dry extract and on the two fractions obtained after aqueous dispersion and centrifugation, enabling separate inspection of the blue water-soluble and green hydrophobic contributions. Based on previous studies on Spirulina fractionation, aqueous processing preferentially solubilizes phycocyanin-rich species, while the hydrophobic fraction is enriched in chlorophyll-related compounds and accessory pigments such as carotenoids [33–35]. In the following, we first discuss the solid-state optical response of these fractions and then use solution-phase measurements and reference compounds to support the spectral assignments [7,19,33–37,49].

As shown in Fig. 1, the solid-state optical response of SP-E reflects the combined contributions of its blue and green fractions. The diffuse reflectance spectrum of the whole extract (Fig. 1a) shows an intermediate behavior between those of the isolated blue and green powders (Figs. 1b,c), consistent with the visual appearance of the non-separated material. The corresponding CIE 1931 chromaticity coordinates, reported in Table S1, quantitatively capture these color differences. Solid-state photoluminescence further highlights the coexistence of distinct emissive channels (Figs. 1d–f), with emission clearly observable under UV excitation. The dominant excitation window associated with red/far-red emission lies in the 575–630 nm region for all samples. The blue fraction exhibits a broader emission peaking at ~685 nm with a shoulder around 735 nm, while the green fraction shows a more defined far-red band centered at ~735 nm. SP-E retains both contributions, indicating the simultaneous presence of blue- and green-derived emissive states. The persistence of a far-red feature in the blue fraction suggests minor residual hydrophobic pigments physically associated with the hydrophilic component, which can be more readily detected by photoluminescence than by diffuse reflectance. To support these assignments, the same fractions were analyzed in solution (blue fraction in water and green fraction in methanol), as reported in Fig. 2.

Figs. 2a–c illustrate the absorption and emission characteristics of the blue aqueous supernatant. The absorption spectrum (Fig. 2a)

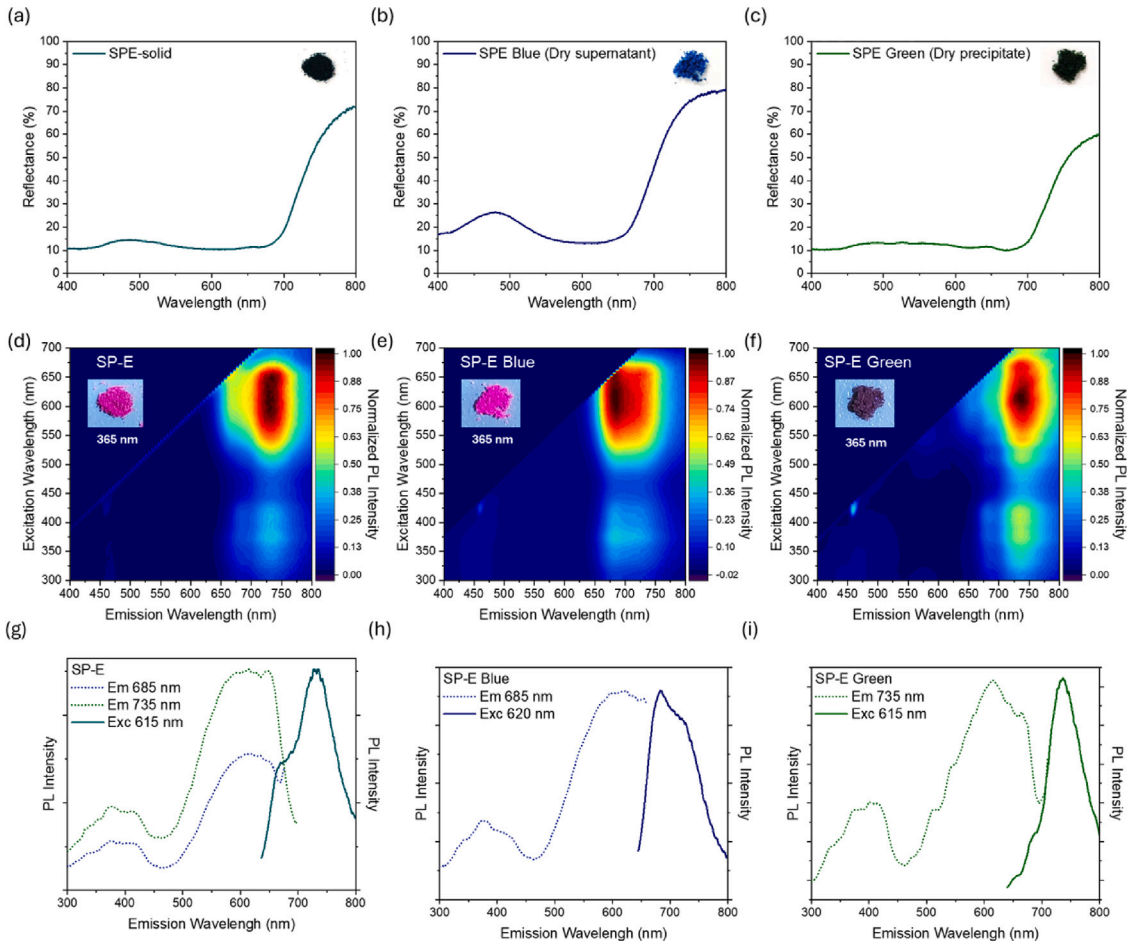


Fig. 1. Optical properties of the Spirulina extract SP-E and its separated blue and green fractions in the solid state. (a-c) Diffuse reflectance spectra of (a) SP-E, (b) the blue fraction, and (c) the green fraction; photographs of the powders under visible light are shown as insets. (d-f) Excitation-emission maps (EEMs) of (d) SP-E, (e) the blue fraction, and (f) the green fraction; photographs under UV illumination (365 nm) are reported as insets. (g-i) Representative excitation and emission spectra extracted from the EEMs of (g) SP-E, (h) the blue fraction, and (i) the green fraction.

shows the typical phycocyanin-related band at 620 nm responsible for the blue coloration [7,19,33–35,49]. The emission spectrum (Fig. 2b) features a broad band centered at 645 nm with a weak shoulder near 700 nm, characteristic of phycocyanin/phycocyanobilin-related emission [7,49], with a quantum yield of 20.1% under excitation at 620 nm (QY_{620nm}). The excitation spectrum of the main emission peaks at 620 nm, while weaker excitation channels are present in the near-UV. Excitation at 410 nm reveals an additional faint band at ~475 nm, attributed to intrinsic protein-related fluorescence. These features are summarized by the excitation–emission map (Fig. 2c), whose inset shows the magenta luminescence observed under 405 nm laser excitation.

The assignment of the aqueous fraction to phycocyanin and phycocyanobilin-related species was further supported by comparison with a purified phycocyanin standard measured under identical conditions (Figure S1), ATR-FTIR analysis of the SP-E blue fraction and phycocyanin standard (Figure S2), and complementary ^{1}H NMR measurements (Figure S3). In particular, the optical spectra of the aqueous SP-E fraction closely reproduced the main absorption and emission signatures of the purified phycocyanin reference, although with slightly broader features and lower apparent purity, as expected for a minimally purified natural extract. The ^{1}H NMR spectrum of the water-soluble SP-E fraction showed spectral features consistent with the purified phycocyanin reference, including resonances in the 3.90–3.85 ppm region and around 5.2 ppm. These signals are compatible with methyl groups on sp^2-hybridized carbons and vinyl-related features associated with the phycocyanobilin chromophore within the phycocyanin scaffold. Additional partially resolved resonances in the 3.80–3.46 ppm region further support the presence of phycocyanin/phycocyanobilin-related components. Together, these data support the dominant contribution of phycocyanin/phycocyanobilin-related species to the optical response of the aqueous fraction. Although the aqueous fraction is dominated by phycocyanin/phycocyanobilin-related signatures, minor chlorophyll-derived contributions cannot be excluded. The ^{1}H NMR spectrum of the water-soluble SP-E fraction also displayed weak resonances in the 5.45–5.30 ppm region, which may indicate minor chlorophyll-derived contributions retained in the aqueous fraction. This observation is consistent with the residual far-red emissive component detected in the solid-state blue fraction and further confirms that the fractionation step enriches, but does not fully purify, the phycocyanin-rich component.

The apparent purity of the phycocyanin-rich aqueous fraction was evaluated using the A_{620}/A_{280} ratio, commonly employed for phycocyanin preparations, where the 620 nm band is associated with the phycocyanin chromophore and the absorbance at 280 nm mainly reflects protein aromatic residues and other UV-absorbing components [47,50]. According to literature classifications [2,3,47,51], samples with $A_{620}/A_{280} > 0.7$ are considered food grade, while values above 4.0 are considered analytical grade. The purified phycocyanin reference exhibited $A_{620}/A_{280} = 2.85$, whereas the aqueous SP-E fraction showed $A_{620}/A_{280} = 0.57$, indicating moderate apparent purity of the hydrophilic fraction, close to the lower bound of the food-grade range.

To assess the reproducibility of this hydrophilic phycocyanin-rich fraction, three independently prepared SP-E batches were compared

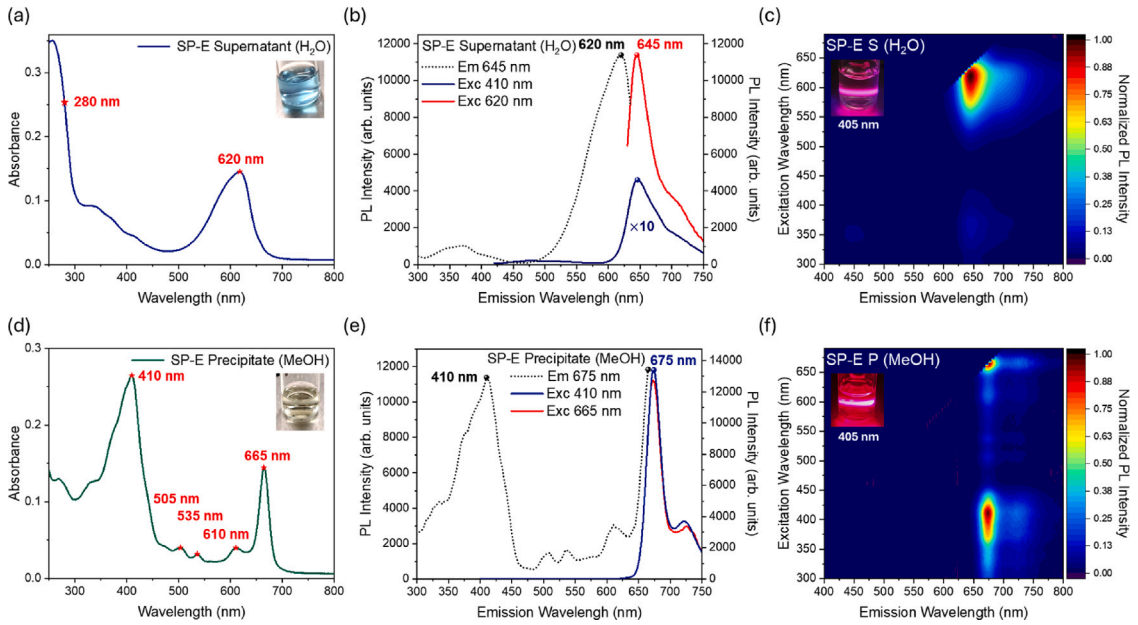


Fig. 2. (a-c) Absorption and emission properties of the aqueous Spirulina extract SP-E supernatant. (a) Absorption spectrum with the characteristic 620 nm band (inset: photograph of the blue aqueous solution under visible light). (b) Emission spectra under excitation at 410 nm (blue line) and 620 nm (red line), compared with the excitation spectrum of the main emission (black dotted line). (c) Excitation-emission map (EEM) and photograph of the bright magenta luminescence under 405 nm laser excitation (inset). (d-f) Optical properties of the methanolic SP-E fraction obtained from the green precipitate. (d) Absorption spectrum showing the typical chlorophyll *a* derivatives features with the Soret and Q-bands (inset: photograph of the green methanolic solution under visible light). (e) Emission spectra under excitation at 410 nm (blue line) and 665 nm (red line) with the excitation spectrum of the main emission (black dotted line). (f) Corresponding EEM and photograph of the bright red luminescence under 405 nm laser excitation (inset).

by UV–vis absorption spectroscopy in water (Figure S4a). All batches retained the characteristic phycocyanin-related absorption band at approximately 620 nm and the same main spectral profile, indicating that the phycocyanin-related optical signature was preserved across preparations. Differences were mainly observed in the relative intensity of the 620 nm band and in the A_{620}/A_{280} ratio, which ranged from 0.38 to 0.57. Therefore, this comparison primarily reflects variations in the relative amount and apparent purity of the hydrophilic phycocyanin-rich fraction, rather than changes in the overall pigment-family composition of the full extract. In particular, the variation in A_{620}/A_{280} is consistent with different contributions from proteinaceous/aromatic UV-absorbing components and other co-extracted species in the aqueous fraction.

The optical response of the methanolic solution obtained from the green precipitate is shown in Figs. 2d–f. The absorption spectrum (Fig. 2d) features an intense Soret band and lower-energy Q-bands, which are characteristic of chlorophyll-related tetrapyrrolic chromophores and arise from π–π^* transitions of the porphyrin macrocycle [1,52]. The sample exhibits intense red emission with a quantum yield of 22.2% under excitation at 665 nm (QY_{665nm}), peaking at 675 nm with a shoulder at ~720 nm (Fig. 2e). The excitation profile closely follows the absorption spectrum, with main excitation maxima at 410 nm and 665 nm, and the EEM (Fig. 2f) confirms red-shifted luminescence under 405 nm excitation compared to the aqueous supernatant.

These spectroscopic features are consistent with the presence of chlorophyll-derived species in the green hydrophobic fraction. Here, the term chlorophyll-derived species refers to chlorophyll *a*-related tetrapyrrolic pigments and conversion/degradation products commonly reported in Spirulina extracts, including pheophytin *a*, pheophorbide *a*, and related derivatives, often coexisting with accessory carotenoids. This interpretation is supported by previous chromatographic studies of Spirulina extracts, where pheophytin *a*, pheophorbide *a*, and related chlorophyll-derived compounds were identified in hydrophobic or precipitated fractions [33–36].

Comparison with a purified chlorophyll *a* standard provided further support for this assignment (Figure S1). The methanolic fraction is not fully coincident with pure chlorophyll *a*, as expected for a minimally purified natural extract, but shows comparable absorption and excitation–emission features. Consistent with this assignment, methanolic extracts obtained from three independently prepared SP-E batches showed highly similar UV–vis spectral profiles, with conserved Soret and Q-band features characteristic of chlorophyll-derived species and only moderate variations in the relative intensity of the red-region band (Figure S4b). This behavior is consistent with the coexistence of multiple chlorophyll-derived species rather than a single pure pigment. In particular, chlorophyll *a* can undergo conversion under the effect of temperature, light, or hydrolytic processes, leading to derivatives such as pheophorbide *a* and pheophytin *a*. Literature reports based on HPLC analysis further indicate that, following aqueous centrifugation, the precipitated fraction can be mainly composed of chlorophyll-related compounds and, to a lesser extent, carotenoids [33]. The absorption features reported for these species are consistent with those observed in our system [33].

NMR analysis provided complementary qualitative support for the presence of chlorophyll-related contributions (Figure S3). Signals in the 6.32–6.20 ppm region, attributable to vinyl residues characteristic of chlorophyll-related species, were observed in the SP-E fractions, although other diagnostic regions were weak or not clearly resolved. Therefore, the NMR data support the presence of chlorophyll-related contributions but do not allow unambiguous identification of individual chlorophyll derivatives. Overall, the optical and NMR analyses indicate that the green fraction is governed by a mixture of chlorophyll-derived chromophores rather than by pure chlorophyll *a* alone.

To gain further insight into emissive dynamics, time-resolved photoluminescence (TR-PL) measurements were performed under 350 nm excitation. The aqueous supernatant exhibited two emission components in the nanosecond regime (Figure S5 and Tab. S2). A dominant band at ~440 nm decayed biexponentially (1.0 ns and 8.9 ns; average lifetime 7.4 ns), with a ~0.7 ns rise component comparable to the

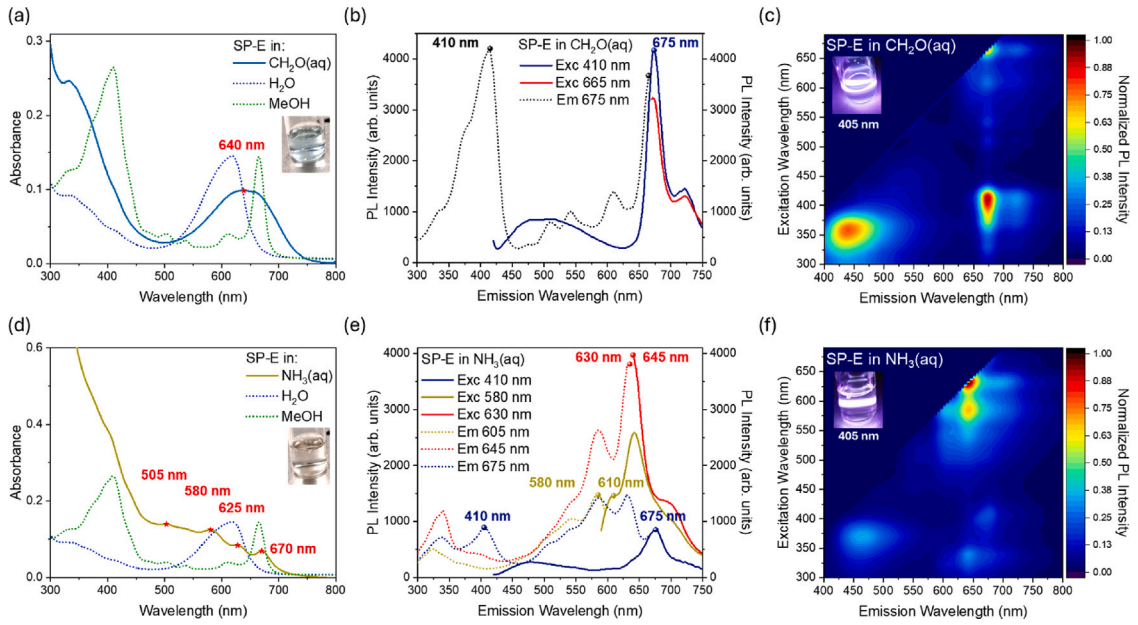


Fig. 3. (a-c) Interaction of SP-E with aqueous CH_2O: (a) absorption spectrum compared to the reference in water and methanol (inset: blue–green solution); (b) emission spectra at 410 nm (blue line) and 665 nm (red line), together with the excitation spectrum of the main emission at 675 nm (black dotted line); (c) excitation-emission map (EEM) and photograph of the violet luminescence under 405 nm laser excitation (inset). (d-f) Interaction of SP-E with aqueous NH_3: (d) absorption spectrum compared to the reference in water and methanol (inset: yellow solution); (e) emission spectra under excitation at 410 nm (blue line), 580 nm (gold line), and 630 nm (red line), with excitation spectra recorded at 645 nm (red dotted line) and 675 nm (blue dotted line); (f) corresponding EEM and photograph of violet luminescence under 405 nm laser excitation (inset).

instrument response and therefore taken as the uncertainty limit. This contribution is attributed to protein-backbone fluorescence, typically masked in steady-state spectra by the dominant chromophore emission. A weaker emission centered at ~630 nm, assigned to the phycocyanin chromophore, followed a monoexponential decay with a lifetime of 1.3 ns, consistent with reported values (1–2 ns) [53–55]. The methanolic fraction showed an analogous dual-emission behavior: a blue band at 435 nm with biexponential decay (0.9 ns and 7.5 ns; average 6.8 ns) and a red band at ~670 nm with a monoexponential lifetime of 4.5 ns, consistent with chlorophyll-derived relaxation pathways [56].

Transient absorption (TA) measurements (Figure S6) were carried out under 350 nm excitation to probe excited-state dynamics of the separated fractions on the nanosecond time scale. For the aqueous blue supernatant, TA spectra are dominated by a broad positive excited-state absorption (ESA) across the visible range, peaking at ~660 nm. The signal decays slowly, with a residual contribution persisting beyond the 8 ns temporal window (Figure S6c), suggesting the formation of long-lived photoexcited species likely stabilized within the protein–chromophore environment. The broad ESA is consistent with overlapping excited-state transitions from multiple phycobilin chromophores or conformational sub-ensembles and may involve slow structural reorganization and/or triplet-like states [12,13]. In contrast, the green fraction in methanol exhibits a pronounced negative band centered at ~665 nm, coincident with the steady-state absorption maximum and assigned to ground-state bleaching (GSB). Two additional positive ESA features appear around 475 nm and 620 nm and decay on the nanosecond time scale (Figure S6f), consistent with chlorophyll *a*–related chromophores and structurally similar conjugated systems [57,58].

Overall, steady-state and time-resolved measurements show that SP-E combines phycocyanin/phycocyanobilin-related and chlorophyll-derived optical signatures whose relative contributions depend on the chemical environment and on pigment–protein interactions. This intrinsic photophysical heterogeneity provides a basis for wavelength-selective and colorimetric readout strategies that are exploited in the following sections.

3.2. Optical response in formaldehyde and ammonia aqueous solutions

To assess the optical responsiveness of the Spirulina-derived extract under chemically aggressive aqueous conditions, we investigated its interaction with aqueous ammonia (NH_3(aq), 10% v/v) and aqueous formaldehyde (CH_2O(aq), 15% v/v). These media were selected because they can perturb the hydrophilic phycocyanin-rich component, whose extraction and optical response are favored by the aqueous environment, while also allowing possible changes in the relative contribution of chlorophyll-derived species to be evaluated. For this purpose, 1 mg of SP-E was dispersed in 3 mL of each medium, briefly sonicated, and centrifuged to remove insoluble residues. After treatment, the residual solids appeared blue in aqueous CH_2O and green in aqueous NH_3, indicating distinct solubilization and interaction behavior. The corresponding supernatants were analyzed spectroscopically (Fig. 3).

In aqueous formaldehyde, the absorption spectrum of SP-E (Fig. 3a) shows a marked modification compared with water, with a visible color change from blue to blue–green. This variation mainly arises from broadening and red-shifting of the phycocyanin-related band from 620 to approximately 640 nm, together with enhanced absorbance in the near-UV region (300–400 nm). Comparison with reference spectra of SP-E in water and methanol indicates an increased relative contribution of chlorophyll-derived species. Consistently, the emission spectrum (Fig. 3b) closely resembles that of the methanolic green fraction, exhibiting a dominant red band centered at 675 nm and an excitation profile similar to that of chlorophyll-rich samples. Compared with methanol, a stronger blue–violet emission component is observed upon deep-blue excitation, slightly red-shifted toward ~500 nm, and is attributed to protein-related fluorescence, as confirmed by the excitation–emission map (Fig. 3c).

Overall, the optical response in aqueous CH_2O is consistent with reduced contribution and perturbation of the phycocyanin-rich component, which weakens the native 620 nm signature and enhances the relative visibility of chlorophyll-derived features. Control experiments on the separated fractions dispersed in aqueous CH_2O (Figure S7) support this interpretation: the blue fraction retains its characteristic phycocyanin-related emission under red excitation while showing

only weak chlorophyll-related features under blue excitation, whereas the green fraction displays the expected chlorophyll-derived spectral pattern in both absorption and luminescence.

A qualitatively different response was observed in aqueous ammonia. Upon dispersion, the solution turned yellow, reflecting a substantial reorganization of the absorption spectrum (Fig. 3d). In addition to enhanced near-UV absorption, multiple bands emerged in the visible region at approximately 505, 580, 625, and 670 nm, indicating the coexistence of several chromophoric contributions. The bands at 505 and 670 nm are consistent with chlorophyll-derived absorption, while the feature at 625 nm is associated with the phycocyanin-related contribution. The additional band at 580 nm, absent under neutral conditions, suggests modification of the phycocyanin/protein chromophore environment under basic conditions, possibly involving deprotonation, conformational changes, or partial denaturation effects [5–7]. Excitation-dependent emission measurements (Fig. 3e) reveal three main emissive channels centered at approximately 610, 645, and 675 nm. The latter two are assigned to phycocyanin-related and chlorophyll-derived contributions, respectively, while the 610 nm emission, preferentially excited at 580 nm, is tentatively attributed to modified phycocyanin/phycocyanobilin-related species, whose emission has been reported in this spectral region [8,9,13,59]. These features are summarized by the excitation–emission map in Fig. 3f, which also shows that near-UV excitation produces violet emission under 405 nm irradiation.

Additional insight is provided by control experiments on the separated fractions under identical basic conditions (Figure S7). The green fraction retains characteristic chlorophyll-derived absorption and emission, dominated by a band at ~675 nm. In contrast, the blue fraction exhibits two emissive components centered at approximately 610 and 645 nm, supporting the assignment of the newly emerging 610 nm channel to the phycocyanin-containing fraction. The selective enhancement of this channel in ammonia is consistent with partial protein denaturation or modification of the local chromophore environment, leading to the coexistence of native and altered phycocyanin-related states.

The comparison between formaldehyde and ammonia thus highlights two distinct interaction mechanisms. In aqueous CH_2O, the optical response is dominated by attenuation of the phycocyanin-related contribution and by the relative enhancement of chlorophyll-derived features. In contrast, aqueous NH_3 induces a more disruptive interaction, involving both the suppression of native phycocyanin signatures and the emergence of additional emissive channels associated with modified phycocyanin/phycocyanobilin-related species. This distinct spectroscopic fingerprint provides a basis for discriminating between these two chemically aggressive aqueous environments.

Based on these solution-phase results, SP-E was then incorporated into a photocurable PEGDA matrix to evaluate whether its chemically induced optical responsiveness could be translated to the solid state. Particular attention was devoted to identifying photopolymerization conditions that enable effective curing while preserving the characteristic phycocyanin/phycocyanobilin-related and chlorophyll-derived optical signatures of the extract. The effect of the photoinitiator/SP-E ratio on curing behavior and optical stability is discussed in the following section.

3.3. Photopolymerization process and optical effect of photoinitiator/SP-E ratio

SP-E was incorporated into a PEGDA700 (P700) matrix via photopolymerization to translate its optical responsiveness into a solid polymeric material. The formulation combined the hydrophilic PEGDA700 monomer with the water-compatible photoinitiator BAPO-OH, enabling the inclusion of a limited amount of water to facilitate SP-E dispersion. Because both SP-E and the photoinitiator absorb in the near-UV/visible range, their relative concentrations were expected to influence both curing kinetics and the final optical appearance of the materials.

To evaluate the effect of SP-E loading, a first series of formulations containing 1, 5, and 10 phr of SP-E at a fixed photoinitiator content of 0.5 phr was investigated under identical irradiation conditions (phr denotes parts per hundred parts of resin by weight). The corresponding photorheological curves of the storage modulus (*G'*) are shown in Fig. 4a. At 1 phr of SP-E, curing proceeded rapidly, reaching a plateau within approximately 5 s; however, the resulting disks exhibited a color shift from blue to a lighter green tone, with a partially discolored central region likely associated with locally higher irradiation intensity. Increasing the dye content to 10 phr significantly slowed down the curing process and led to incomplete polymerization, producing films with inhomogeneous color and visible SP-E aggregation. Among the tested formulations, 5 phr of SP-E provided a suitable balance between curing efficiency and optical preservation under the selected irradiation conditions, yielding cured films with a more homogeneous visual appearance and retained pigment-related coloration.

To further clarify the origin of the observed color variations, the influence of the photoinitiator concentration was examined at fixed SP-E content (1 phr). As shown in Fig. 4b, efficient polymerization was achieved for all tested BAPO-OH concentrations (0.1, 0.5, and 1 phr). However, when the photoinitiator content exceeded 0.1 phr, the cured disks consistently displayed a color change from bright blue to pale green, accompanied by a slightly bleached central area. A comparable behavior was observed under lamp-assisted photopolymerization, where color variations became evident immediately after irradiation once the photoinitiator/SP-E weight ratio exceeded approximately 0.1 (Figure S8). These observations suggest that high photoinitiator/SP-E ratios can perturb the phycocyanin-related chromophore during curing, leading to attenuation of the blue absorption and increased relative contribution of green–yellow components.

To assess whether the color change observed at high photoinitiator/SP-E ratio is consistent with oxidative perturbation of the phycocyanin-rich component, control experiments were performed by exposing SP-E to a model oxidant, H_2O_2. Fig. 5a shows the absorption spectra of SP-E in pure water and after addition of 1.5% H_2O_2. While the pristine sample displays the characteristic phycocyanin-related band at 620 nm, this feature is strongly attenuated upon oxidation, accompanied by the emergence of new absorption shoulders around 505, 610, and 665 nm. These spectral changes are consistent with perturbation/degradation of the phycocyanin/phycocyanobilin-related chromophore and increased relative visibility of additional chromophoric species, including chlorophyll-derived contributions. This spectral profile resembles that observed for SP-E in aqueous ammonia, suggesting that oxidative and basic environments induce a phenomenologically similar attenuation of the phycocyanin-related optical features and redistribution of chromophoric contributions.

The corresponding normalized photoluminescence spectra (Fig. 5b) further support this interpretation. Under 405 nm excitation, the emission color changes from magenta in pure water to lilac in the presence of H_2O_2, reflecting both an increased blue contribution and a red-shift of the dominant emission toward 675 nm, consistent with enhanced relative contribution of chlorophyll-derived species. When excited at 600 nm, the oxidized sample exhibits coexisting emission contributions associated with phycocyanin/phycocyanobilin-related and chlorophyll-derived chromophores, confirming that oxidative conditions modify the relative optical contributions of the pigment families.

To further clarify the role of radical species generated during photopolymerization, additional solution-phase experiments were carried out by mixing SP-E with the photoinitiator BAPO-OH in aqueous dispersion and recording absorption spectra before and after UV irradiation (Figure S9a–c). Upon irradiation, a progressive color change and a spectral evolution analogous to that induced by H_2O_2 were observed. This similarity suggests that radical species generated during BAPO-OH

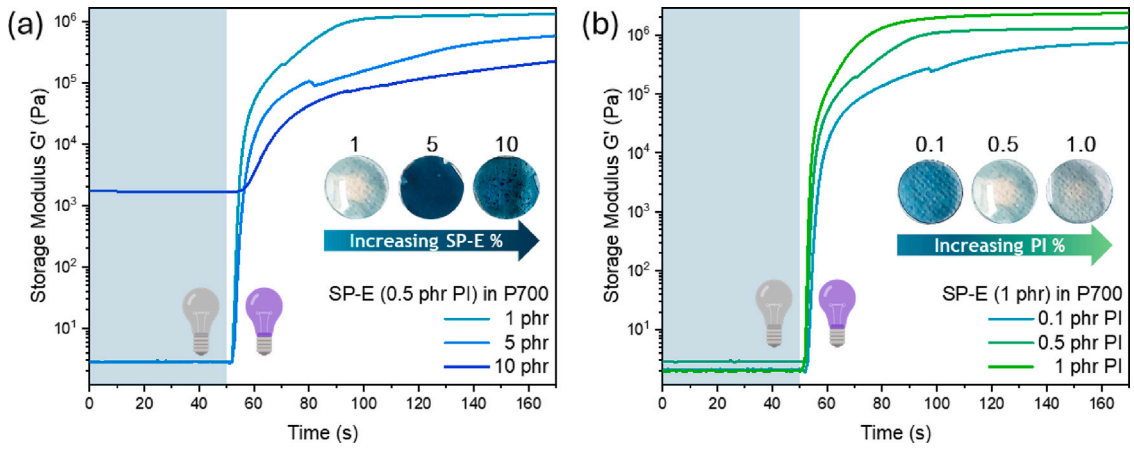


Fig. 4. Photorheological characterization of SP-E-PEGDA formulations. (a) Storage modulus (*G'*) as a function of irradiation time for samples containing 1, 5, and 10 phr of SP-E at fixed photoinitiator (PI) content (0.5 phr). (b) Storage modulus (*G'*) as a function of irradiation time for samples containing 0.1, 0.5, and 1 phr of PI at fixed SP-E content (1 phr). Insets: photographs of the corresponding cured disks.

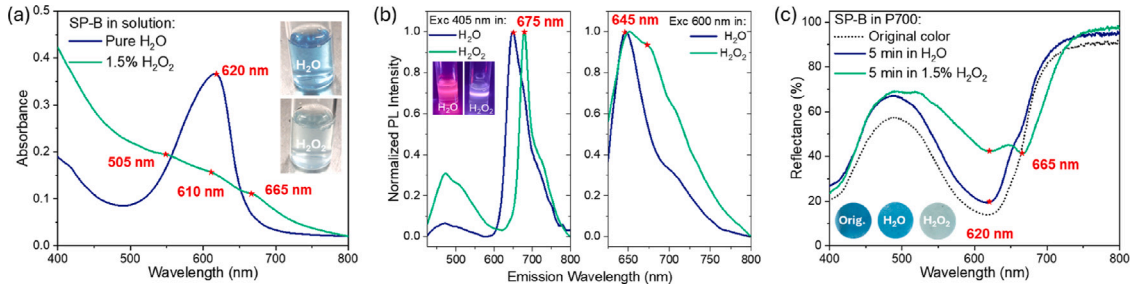


Fig. 5. (a) Absorption spectra of SP-E in pure water (inset: blue solution) and in 1.5% H_2O_2 (inset: green solution). (b) Normalized photoluminescence spectra under excitation at 405 nm and 600 nm, with insets displaying the emission colors under 405 nm laser illumination (magenta in water, lilac with H_2O_2). (c) Reflectance spectra of SP-E-PEGDA700 films after immersion in water and in 1.5% H_2O_2 (inset: photographs of the films).

photolysis can promote perturbation or degradation of the pigment–protein scaffold, leading to redistribution of chromophoric contributions comparable to that observed under externally applied oxidizing conditions.

To verify whether this behavior was specific to BAPO-OH, analogous experiments were carried out using LAP as an alternative radical-generating photoinitiator (Figure S9d–f). Upon irradiation, the SP-E/LAP system also exhibited strong attenuation of the 620 nm phycocyanin-related band and visible bleaching, supporting the involvement of radical-mediated pigment perturbation. Nevertheless, other contributions, such as oxygen-mediated oxidation, local thermal effects, or changes in the local chromophore environment, cannot be fully excluded. Therefore, radical-mediated perturbation is considered a plausible mechanism rather than a definitive assignment.

A similar trend was observed in solid SP-E–P700 films. As shown in Fig. 5c, immersion in water for 5 min produced only a modest decrease in the 620 nm band, consistent with matrix-controlled hydration effects and changes in optical scattering/path length rather than extensive dye release. In contrast, immersion in 1.5% H_2O_2 led to the appearance of a distinct band at 665 nm and a visible color transition from light blue to green. This interpretation is consistent with the water-immersion leaching experiments as discussed below, which showed negligible mass loss and no quantifiable release of SP-E into the surrounding aqueous medium.

Overall, these findings highlight the role of photopolymerization conditions in determining both curing kinetics and the optical stability of SP-E within the polymer matrix. High photoinitiator/SP-E ratios lead to pronounced attenuation of the phycocyanin-related contribution and shift the optical balance toward chlorophyll-derived and green–yellow components, resulting in a blue-to-green color transition. This behavior is consistent with radical-mediated perturbation or degradation of the phycocyanin/phycocyanobilin-related chromophore, although additional effects such as oxygen-mediated oxidation, local thermal changes, or chromophore redistribution within the forming network may also contribute. A careful balance between photoinitiator and SP-E concentrations is therefore required to achieve effective polymerization while preserving the desired optical response. In this work, formulations with a photoinitiator/SP-E ratio of approximately 1:10 by weight provided a suitable balance between curing efficiency and retention of the characteristic SP-E optical signature under the selected irradiation conditions. These insights are essential for the rational integration of SP-E into photopolymer-based optical indicators and additive-manufacturing architectures.

3.4. Colorimetric response of SP-E–PEGDA films in liquid and vapor/headspace environments

On the basis of the solvent-dependent optical behavior observed in solution, we next investigated whether the chemically induced spectral changes of SP-E could be translated to a solid polymeric matrix. SP-E was incorporated into a PEGDA700 network via photopolymerization, yielding optically active disks with a diameter of approximately 2 cm and a thickness of 0.2 mm. Films were immersed for 30 min in distilled water, 98% methanol, 15% aqueous formaldehyde, and 10% aqueous ammonia, and analyzed by diffuse-reflectance spectroscopy.

Although solution-phase experiments showed both colorimetric and luminescent variations, the luminescent response of bulk-photopolymerized films is strongly affected by sample thickness, light penetration depth, scattering, and local SP-E distribution. Diffuse-reflectance colorimetry was therefore selected as the primary readout

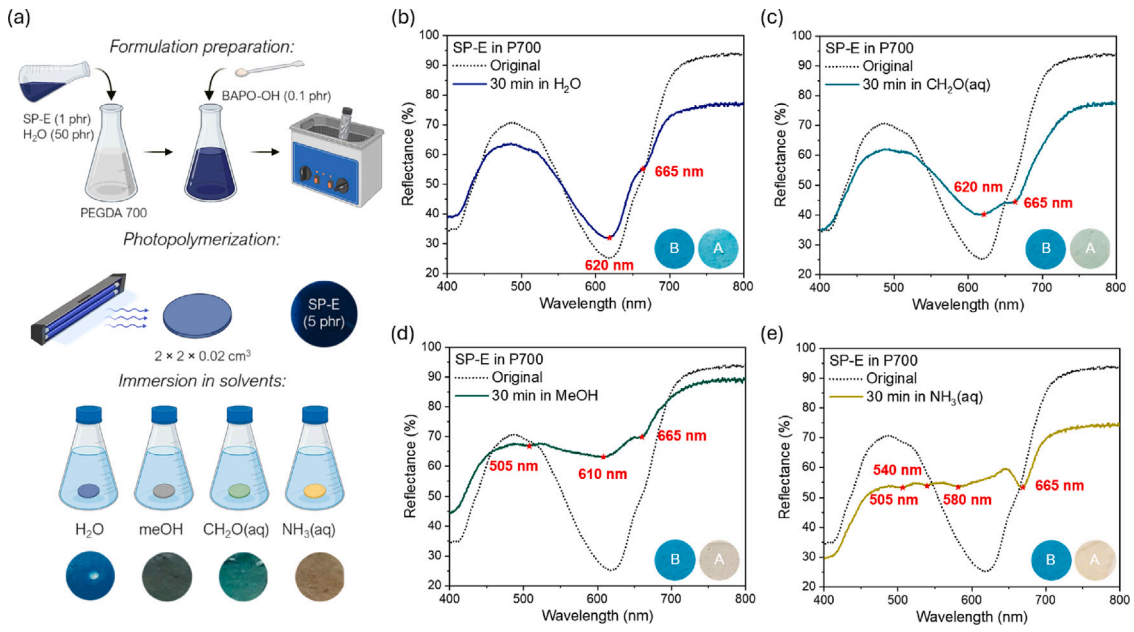


Fig. 6. Colorimetric response of SP-E-PEGDA films after immersion for 30 min in different solvents. (a) Experimental scheme and photographs of disks with higher SP-E loading (5 phr) used to emphasize color differences. Created in BioRender. C. (2026) https://BioRender.com/d6uy876. (b–e) Reflectance spectra and corresponding disk images (1 phr, insets) before (B) and after (A) immersion in (b) water, (c) aqueous formaldehyde, (d) aqueous ammonia, and (e) methanol. In all plots, the reflectance spectrum of the pristine disk is shown for comparison (black dotted line).

for bulk films. As discussed below, DLP printing can partially mitigate these limitations through layer-wise fabrication, reduced effective optical path length, and improved chromophore accessibility. Fig. 6a shows the experimental procedure and macroscopic color variations using disks with higher SP-E loading to emphasize visual differences, whereas the reflectance analyses were performed on lower-loading films to improve film uniformity and reduce SP-E aggregation (insets of Figs. 6b–e).

Immersion in water (Fig. 6b) was first examined to evaluate the stability of the hydrophilic phycocyanin-related contribution within the polymer matrix. After 30 min, the reflectance spectrum showed attenuation of the 620 nm band, accompanied by a visible color shift from intense to lighter blue. A general decrease in reflectance across the visible region was also observed, consistent with increased opacity due to swelling of the PEGDA-based network in aqueous media.

To distinguish between pigment release and matrix-induced optical effects, swelling, mass-loss, leaching, and apparent optical-retention measurements were performed under the same water-immersion conditions (Table S3 and Figure S10). Gravimetric analysis showed significant water uptake, with a swelling ratio of approximately 70%–75%, while mass loss after re-drying was negligible. Possible release of the hydrophilic phycocyanin-related fraction was evaluated by monitoring the absorbance of the surrounding aqueous medium at 620 nm. The measured absorbance values were very low and comparable to the blank/calibration intercept, indicating that the released SP-E concentration was below the quantification limit of the UV–vis method.

The optical signal of the films before and after immersion was compared by converting diffuse-reflectance data into reflectance-derived apparent absorbance at 620 nm. After 30 min immersion, the films retained approximately 75% of the initial phycocyanin-related optical signal, corresponding to an attenuation of about 25%. Since this attenuation was not accompanied by measurable SP-E release or gravimetric mass loss, it is mainly attributed to swelling-induced matrix effects, including changes in opacity, scattering, optical path length, local hydration, and chromophore accessibility, rather than to extensive pigment leaching.

Therefore, water immersion primarily affected the phycocyanin-related optical contribution through matrix-controlled hydration effects, while the chlorophyll-derived component remained largely unaffected, as indicated by the persistence of the reflectance minimum at 665 nm.

In aqueous formaldehyde (Fig. 6c), the reflectance spectrum retained the phycocyanin-related feature at 620 nm but exhibited the appearance of an additional minimum around 665 nm, attributed to chlorophyll-derived species. This spectral evolution is consistent with solution-phase observations and results in a characteristic blue–green coloration of the films. The optical response in formaldehyde is therefore dominated by attenuation of the phycocyanin-related contribution, which enhances the relative visibility of the chlorophyll-derived fraction within the polymer matrix.

In methanol (Fig. 6e), SP-E-PEGDA films underwent a color change from bright blue to gray. The corresponding reflectance spectrum confirmed the loss of the phycocyanin-related absorption and the persistence of weak features in the red region, similar to those observed for SP-E in methanolic solution. A faint shoulder around 610 nm suggests a minor contribution from residual or modified phycocyanin/phycocyanobilin-related species. These observations indicate that methanol attenuates phycocyanin-related signatures while increasing the relative visibility of chlorophyll-derived contributions within the polymer matrix.

A comparable yet more pronounced modification was observed upon immersion in aqueous ammonia (Fig. 6d). After treatment, the characteristic phycocyanin-related absorption at approximately 625 nm was strongly attenuated, while multiple features associated with chlorophyll-derived species and phycocyanin/phycocyanobilin-related components emerged. This behavior likely reflects base-induced perturbation of the protein scaffold, leading to attenuation of the native phycocyanin-related absorption channel and the appearance of additional phycocyanin/phycocyanobilin-related signatures in the 580–610 nm region. As a result, the films exhibited a yellow color closely resembling that of SP-E in ammonia solution. In analogy with solution-phase results, ammonia thus induces a stronger and more complex interaction with the phycocyanin-containing fraction compared to formaldehyde.

To further support the spectral assignments within the polymer matrix, control PEGDA films containing purified phycocyanin (PCN) were prepared and exposed to the same liquid environments (Figure S11). In the pristine state, PCN-containing films displayed a phycocyanin-related reflectance feature comparable to that of SP-E-containing films, but did not show the additional red-region contribution expected from the chlorophyll-derived fraction of the full extract. After exposure to methanol and formaldehyde, PCN-containing films did not exhibit a persistent feature at approximately 665 nm, supporting the assignment of this band in SP-E films to chlorophyll-derived species rather than to phycocyanin itself.

Conversely, upon exposure to NH_3(aq), PCN-containing films showed distinct spectral features in the 580–630 nm region. These features are consistent with perturbation of the phycocyanin/phycocyanobilin chromophore and support the attribution of the ammonia-induced bands observed in SP-E films to phycocyanin/phycocyanobilin-related species. Although contributions from minor constituents of the natural extract cannot be completely excluded, the comparison with purified PCN-containing films indicates that the dominant spectral changes can be rationalized in terms of phycocyanin/phycocyanobilin-related and chlorophyll-derived contributions.

To provide a quantitative proof-of-concept for this response, NH_3(aq) was selected as a representative analyte for concentration-dependent measurements. SP-E-PEGDA films were exposed to aqueous NH_3 solutions in the 0%–10% v/v range for 30 min, using the same immersion time adopted for the liquid-response experiments. The diffuse-reflectance spectra were converted into reflectance-derived apparent absorbance values, as described in the Experimental Section, and the optical response was quantified using the normalized ratiometric signal S. This ratiometric index accounts for both attenuation of the phycocyanin-related contribution at 620 nm and the increased relative contribution of the chlorophyll-derived band at 665 nm.

The calibration curve showed a concentration-dependent increase of the ratiometric response in the low-concentration range (Figure S12). The sensitivity, defined as the slope of the linear fit, was 0.24 (% v/v)$^{-1}$. The LOD, calculated using the $3\sigma/m$ criterion, where σ is the standard deviation of the blank response and m is the calibration slope, was estimated to be 0.41% v/v NH_3 after 30 min exposure. This value should be interpreted as an operational detection limit associated with the reflectance-derived ratiometric readout. The response time was evaluated at 10% v/v NH_3 by monitoring the time-dependent evolution of $S(t)$. Since the response showed a sigmoidal approach to a plateau, the data were fitted with a Boltzmann function as an empirical descriptor of the transition. The apparent response time, defined as the time required to reach 90% of the total signal variation, was estimated to be approximately 10 min. It should be noted that the NH_3(aq) response occurs within a hydrated PEGDA network; therefore, the ratiometric changes are governed not only by base-induced perturbation of the phycocyanin-related chromophore, but also by swelling, analyte diffusion, local hydration, and chromophore accessibility.

Except for the NH_3(aq) calibration described above, the responses to formaldehyde and methanol are therefore considered qualitative demonstrations of chemically induced optical responsiveness rather than fully optimized analytical sensing tests. Taken together, the liquid-immersion results show that the optical response of SP-E-PEGDA films is governed by the interplay between intrinsic pigment chemistry and matrix-controlled effects. Water mainly induces swelling-related optical changes with no quantifiable SP-E release, whereas chemically aggressive media such as NH_3(aq), formaldehyde, and methanol produce stronger perturbations of pigment-related spectral features. Since the spectral variations persisted after drying, the resulting color changes should be interpreted as indicator responses rather than fully reversible sensing events under the tested conditions.

To assess the response of SP-E-PEGDA films to volatile chemical environments, samples were exposed in a static headspace configuration (Fig. 7a). Polymer disks were placed in open vials inside sealed vessels containing methanol, 10% aqueous ammonia, or 15% aqueous formaldehyde and kept at room temperature for 24 h.

In contrast to liquid immersion, vapor exposure did not induce visible matrix opacity. All films remained transparent and glossy, as confirmed by the reflectance spectra in Fig. 7b. Comparison with liquid-phase experiments (Figs. 7c–e) revealed that vapor/headspace-induced colorimetric responses qualitatively followed the trends observed after liquid immersion, although with reduced spectral contrast and intensity, consistent with lower effective uptake and diffusion-limited transport.

Specifically, films exposed to methanol vapor (Fig. 7c) and ammonia vapor (Fig. 7e) displayed a dominant reflectance feature at 665 nm, associated with the chlorophyll-rich fraction. The resulting color changes were subtle, with pale gray tones in methanol and faint yellow hues in ammonia. No additional spectral features were detected. In contrast, exposure to formaldehyde vapors (Fig. 7d) produced only a slight lightening of the original blue color, without marked enhancement of the chlorophyll-related band, indicating a weaker interaction under headspace exposure conditions.

These results show that SP-E retains chemically responsive optical behavior after incorporation into a PEGDA matrix and remains responsive to both liquid and vapor/headspace chemical environments. No visible coloration of the surrounding atmosphere or condensate was observed during vapor/headspace exposure, supporting the absence of significant pigment migration under these conditions. While vapor/headspace responses are attenuated compared to direct immersion, owing to lower effective solvent uptake and diffusion constraints, the observed colorimetric changes support the potential of SP-E-PEGDA composites as solid-state indicators for chemically aggressive environments.

However, except for the quantitative NH_3(aq) proof-of-concept analysis reported above, the responses to formaldehyde, methanol, hydrogen peroxide, and vapor/headspace exposure are intended as qualitative demonstrations of chemically induced optical responsiveness, rather than as fully validated analytical sensing tests. Moreover, under the tested conditions, which involved full immersion or exposure to saturated headspace environments, the observed color changes did not fully revert upon simple drying. Therefore, SP-E-PEGDA films are more appropriately described as proof-of-concept optical indicators or dosimetric materials than as fully reversible sensors.

To further assess the persistence of the exposure-induced optical states, the same SP-E-PEGDA samples were re-measured after one year of storage under ambient conditions, without re-exposure to the corresponding media (Figure S13). The pristine SP-E-PEGDA film showed spectral changes after storage, indicating that aging-related effects of the polymer/pigment system may contribute to the long-term optical evolution. Nevertheless, samples previously exposed to NH_3(aq), methanol, and formaldehyde retained distinct post-exposure spectral profiles after one year, confirming that the chemically induced optical states are persistent rather than rapidly reversible. These observations support the interpretation of SP-E-PEGDA films as optical indicators or dosimetric materials under the aggressive exposure conditions investigated here. Future work should address reversibility, selectivity, lower detection limits, and controlled sub-saturated exposure regimes.

3.5. Vat photopolymerization and DLP printing of SP-E-based architectures

Following optimization of the photopolymerization parameters, SP-E-based formulations were processed by projection-based vat photopolymerization/DLP printing to evaluate printability, dimensional agreement with CAD models, and optical functionality. Multiple CAD models were selected to assess representative feature definition, processability of the optimized formulation, and fabrication of architected geometries with optically active behavior.

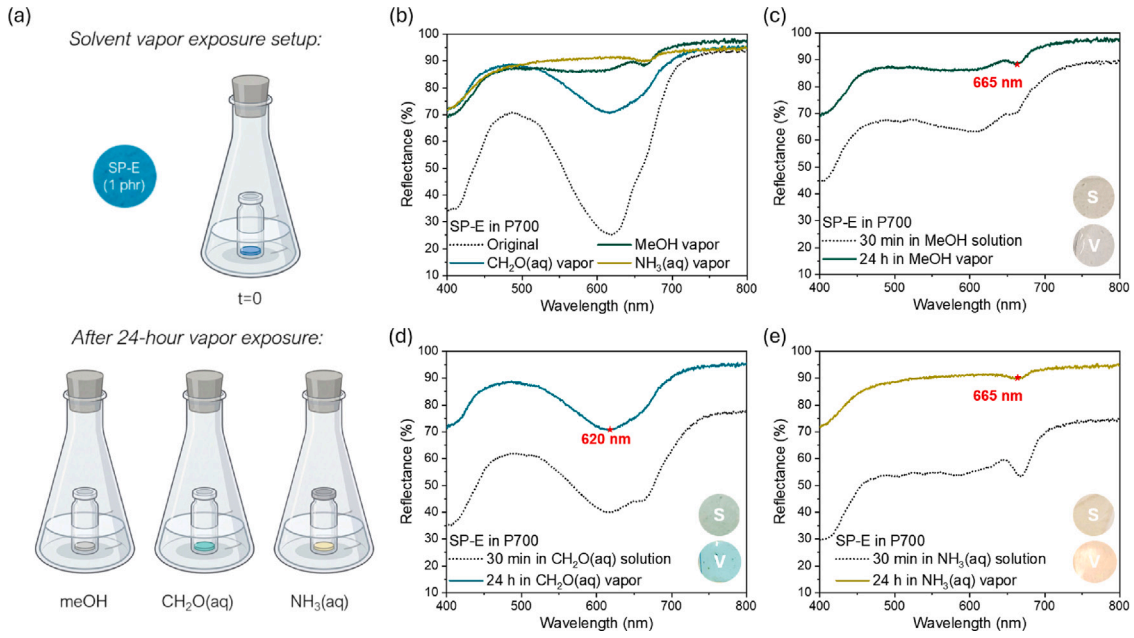


Fig. 7. Colorimetric response of SP-E-PEGDA films upon exposure to solvent vapors for 24 h. (a) Schematic representation of the vapor-exposure setup. Created in BioRender. C. (2026) https://BioRender.com/i8anauk. (b) Reflectance spectra of vapor-exposed films compared to the pristine sample. (c–e) Comparison between reflectance spectra after exposure to liquid solvents (dotted lines) and solvent vapors (solid lines) for (c) methanol, (d) formaldehyde, and (e) ammonia. Insets: photographs of the corresponding films after solvent (S) and vapor (V) exposure.

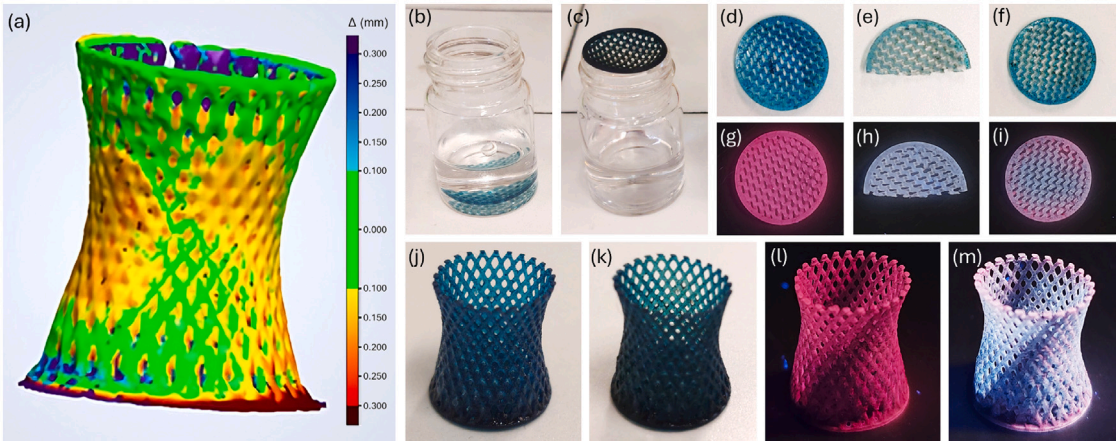


Fig. 8. DLP printing of SP-E-PEGDA architectures and optical response to ammonia exposure. (a) Overlay between the three-dimensional optical scan of a printed lattice structure and the corresponding CAD model; green regions indicate dimensional deviations below 100 μm. (b,c) Experimental setup showing immersion and vapor/headspace exposure conditions for ammonia treatment. (d–f) Visible-light photographs of a 1 phr SP-E printed disk: (d) pristine, (e) after 5 min immersion in aqueous ammonia, and (f) after 30 min exposure to ammonia vapor/headspace. (g–i) Corresponding images under 365 nm excitation, highlighting the luminescent response of the 1 phr disk before and after exposure. (j,k) Complex 3D-printed lattice structure containing 5 phr SP-E under visible light: (j) pristine and (k) after 5 min ammonia vapor/headspace exposure. (l,m) The same structure under 365 nm excitation.

Initial printing trials performed using exposure parameters optimized for the transparent PEGDA700 reference resin resulted in incomplete curing and loss of fine features when SP-E was incorporated, confirming that the chromophoric extract significantly modifies light penetration and curing dynamics. Dedicated optimization of the printing parameters was therefore required. The optimized conditions, corresponding to a 50 μm layer thickness, 4 s normal exposure time, 6 s bottom exposure time, and 8 bottom layers for the 5 phr formulation, enabled the fabrication of complex geometries with good structural integrity.

The role of SP-E in the printing process becomes evident when comparing the SP-E-containing formulation with the transparent PEGDA700 reference resin (Figure S14). In the absence of a light-attenuating additive, excessive light penetration and lateral scattering within the resin vat can promote uncontrolled polymerization and reduced edge definition. Conversely, incorporation of SP-E introduces intrinsic optical absorption that can limit stray-light-induced curing and contribute to printing control. This effect is analogous to that achieved using synthetic light absorbers commonly employed in DLP printing, here explored using a naturally derived multi-pigment extract.

To further evaluate the role of SP-E as a light-attenuating additive, cure-depth measurements were performed as a function of irradiation time and light intensity (Figure S15). The cured thickness increased with both exposure time and irradiance, but deviations from linearity were observed at longer exposure times, indicating that the process progressively shifts from a reaction-limited regime to a light-attenuation-limited regime. At 30 s exposure, the measured curing depths were approximately 1.54 mm at 5.9 mW cm^{-2}, 1.98 mm at 11.8 mW cm^{-2},

and 2.08 mm at 22.7 mW cm^{-2}. The limited increase in final curing depth between 11.8 and 22.7 mW cm^{-2} suggests that increasing photon flux mainly accelerates polymerization kinetics, while the effective curing depth becomes progressively constrained by optical attenuation within the resin.

As an additional DLP-printing benchmark, SP-E-containing test patterns were compared with test patterns printed from brilliant-green-containing formulations used as conventional synthetic absorber references (Figure S16 and Table S4). Both formulations were printed using the Asiga MAX UVX27 system under comparable conditions. This comparison was used to evaluate representative feature definition and dimensional agreement of SP-E-containing formulations relative to a conventional absorber benchmark. The analyzed CAD pattern contained both positive and negative circular geometries, namely raised circular features and recessed holes with nominal diameters of 0.15, 0.20, 0.30, and 0.40 mm. Feature diameters were measured from optical microscopy images, compared with the corresponding nominal CAD values, and reported as mean ± SD.

For the SP-E formulation, both raised features and recessed holes remained close to the CAD dimensions, with absolute deviations generally below 0.02 mm. The corresponding lateral bias values were small, indicating limited dimensional distortion under the selected printing conditions. In the case of raised features, positive lateral bias denotes feature broadening, whereas negative values indicate slight narrowing or underfilling. Conversely, for recessed holes, positive lateral bias indicates hole narrowing or partial closure, while negative values indicate apparent hole enlargement.

Compared with SP-E, the brilliant-green-containing formulation showed larger deviations from the CAD values, particularly for recessed holes. While the raised features printed with brilliant green showed moderate broadening, the recessed holes displayed larger apparent enlargement and poorer edge definition, with the smallest holes being only partially resolved in some regions. Therefore, for the brilliant-green-containing formulation, the values reported for recessed holes should be interpreted as apparent diameters of resolved or partially resolved negative features rather than as ideal circular openings.

This representative feature-size analysis supports the compatibility of SP-E with sub-millimetric feature fabrication by DLP printing and provides a quantitative benchmark against a conventional synthetic absorber. Importantly, the distinction between raised and recessed geometries shows that SP-E enables more faithful reproduction not only of positive features, but also of small negative features, which are particularly sensitive to stray curing and local light propagation. However, SP-E is not presented here as a fully optimized replacement for commercial absorbers; rather, these results demonstrate its proof-of-concept function as a multifunctional natural additive capable of combining optical responsiveness with light-attenuation-assisted printing control.

To assess transferability to a higher-resolution DLP platform, printing experiments were carried out using an Asiga MAX UVX27 system. Representative CAD geometries were fabricated under optimized exposure conditions (Figure S17), supporting the processability of the SP-E-based formulation on this platform. One lattice-based architecture was selected for quantitative dimensional analysis and subjected to three-dimensional optical scanning. Direct overlay with the corresponding CAD model (Fig. 8a) revealed that, for this representative architecture, most of the scanned structure exhibited dimensional deviations below 100 μm, supporting good dimensional agreement between the printed object and the reference design.

Beyond dimensional analysis, the optical response of the printed architectures to ammonia exposure was investigated as a proof-of-concept chemical indication test. Disks containing 1 phr SP-E (Fig. 8) and 5 phr SP-E (Figure S18) were exposed to aqueous ammonia either by immersion for 5 min or by vapor/headspace treatment for 30 min. Under visible light (Fig. 8d–f), the colorimetric variations were modest, consistent with the behavior observed in planar films. In contrast, under 365 nm excitation (Fig. 8g–i), a pronounced modulation of the luminescent emission was observed, indicating that printed architectures enable a visually accessible luminescence-based readout.

To further demonstrate architectural versatility, a complex lattice structure containing 5 phr SP-E was fabricated (Fig. 8j–m). While visible-light inspection revealed moderate chromatic changes upon ammonia vapor/headspace exposure, 365 nm excitation highlighted a clear redistribution of emission intensity across the structure, indicating that luminescence-based chemical indication is preserved in architected 3D geometries.

The more evident luminescent response observed in printed architectures is likely related to combined effects of fabrication pathway, geometry, effective optical path length, and chromophore accessibility. In planar films obtained by bulk photopolymerization, excitation and emission collection can be limited by sample thickness, scattering, and partial confinement of chromophoric species within the bulk. In contrast, the layer-by-layer curing mechanism of DLP printing immobilizes SP-E within thinner layers and may increase the fraction of optically accessible chromophores.

To further investigate the different luminescent responses of bulk-photopolymerized films and DLP-printed samples, both systems were compared by optical microscopy under visible and UV light and by spatially resolved optical measurements (Figure S19). Optical microscopy at 10× magnification revealed different SP-E organization in the two materials. Bulk films displayed localized pigment-rich regions and a less uniform luminescent appearance, whereas printed samples showed a more regular texture associated with the layer-by-layer fabrication process.

Spatially resolved optical measurements performed at different lateral positions showed only moderate variations in the apparent absorbance ratio between the 620 and 665 nm bands, for both sample types. This apparent discrepancy with the microscopy observations is attributed to the different spatial sensitivity of the two techniques: UV–vis measurements probe an averaged optical response over the illuminated area and are therefore less sensitive to small local heterogeneities. Accordingly, the more evident luminescent response of printed architectures cannot be attributed solely to lateral SP-E homogeneity, but is more likely related to the combined effects of layer-wise immobilization, reduced effective optical path length, geometry, and chromophore accessibility.

ATR-FTIR spectroscopy was further used to compare the chemical structure of the liquid formulations and the corresponding cured materials (Figures S20 and S21). For the unloaded PEGDA700 reference, comparison between the liquid resin and the printed sample showed the expected decrease of the acrylate C=C band at 1635 cm^{-1} after printing, consistent with network formation (Figure S20). Analogously, SP-E-containing samples analyzed in the liquid state, after DLP printing, and as bulk-photopolymerized films showed attenuation of the acrylate C=C contribution after curing, while retaining the main PEGDA/P700 network features (Figure S21).

The relative conversion estimated from ATR-FTIR was approximately 85% for unloaded P700, 80% for the SP-E bulk film, and 68% for the SP-E printed object. These values confirm effective network formation in both SP-E-containing systems. The slightly lower conversion observed for the printed SP-E sample is consistent with the light-attenuating role of the extract during layer-by-layer photopolymerization, while the high conversion of the bulk SP-E film indicates that incorporation of the extract does not prevent efficient PEGDA network formation under the selected curing conditions.

Therefore, the different luminescent response observed between bulk and printed samples is not attributed to major changes in polymer chemical structure alone, but rather to combined effects of fabrication pathway, geometry, effective optical path length, layer-wise immobilization, and chromophore accessibility.

Overall, these results support a dual function of SP-E in DLP printing: it acts as a naturally derived light-attenuating additive that contributes to photopolymerization control, and as an active optical component enabling luminescence-based chemical indication in three-dimensional architectures. The cure-depth measurements, comparison with the transparent PEGDA700 reference, and benchmarking against brilliant green support the role of SP-E in attenuating light penetration, although further systematic optimization would be required to fully define lateral resolution limits, edge sharpness, and geometry-dependent overcuring or feature-bias behavior. The integration of sustainable pigment systems with additive manufacturing thus provides a pathway toward multifunctional, bio-derived printed materials with combined structural and optical functionality.

Conclusions

In this work, we systematically investigated the optical response of a Spirulina-derived extract (SP-E) across liquid and solid-state environments, assessing its suitability as a bio-derived, processable optical material. By deliberately preserving the intrinsic compositional complexity of the extract, SP-E combines phycocyanin/phycocyanobilin-related and chlorophyll-derived pigment families whose relative optical contributions can be modulated by solvent polarity, pH, and oxidative environments.

In solution, SP-E exhibited characteristic phycocyanin-related absorption and emission signatures in water, while methanol and aqueous formaldehyde promoted optical responses dominated by chlorophyll-derived features. More disruptive environments, such as aqueous ammonia and oxidative conditions (H_2O_2), induced pronounced spectral reorganization associated with attenuation of the phycocyanin-related contribution and increased visibility of additional chromophoric species. These transformations resulted in measurable blue-to-green/yellow color changes, highlighting the environmental sensitivity of the extract.

When embedded into PEGDA700 via photopolymerization, SP-E retained chemically responsive colorimetric behavior under both liquid-phase and vapor/headspace exposure. In the solid state, however, the response was governed not only by intrinsic pigment chemistry, but also by matrix-controlled effects such as swelling, diffusion, pigment retention, optical thickness, and chromophore accessibility. A quantitative proof-of-concept response was obtained for aqueous NH_3, with the resulting detection limit interpreted as an operational value associated with the reflectance-derived ratiometric readout. Under the concentrated immersion and saturated-vapor conditions investigated here, the materials are therefore better described as optical indicators or dosimetric materials rather than fully reversible sensors. The photoinitiator/SP-E ratio was also identified as a critical design parameter: high photoinitiator loading attenuated the phycocyanin-related signature, whereas selected formulations enabled effective polymerization while better preserving the characteristic SP-E optical signature.

Beyond photopolymerized films, SP-E was integrated into DLP 3D-printing formulations, enabling the fabrication of optically active microstructures with representative sub-millimetric feature definition and dimensional agreement with CAD models. In this context, the extract acted as a naturally derived light-attenuating additive that contributed to printing control, while retaining its optical responsiveness. Printed architectures also exhibited a visually accessible luminescence-based response, indicating that fabrication pathway, geometry, and chromophore accessibility influence the final optical readout.

Overall, this study positions Spirulina-derived extracts as multifunctional, bio-based additives that combine environmental optical responsiveness with compatibility with photopolymer processing and additive manufacturing. By exploiting extract complexity rather than eliminating it, this approach offers a sustainable route toward pigment-based optical indicators and bio-derived photonic architectures, while providing a foundation for future optimization in terms of permeability, selectivity, extract standardization, controlled exposure regimes, and reversibility under milder conditions.

CRediT authorship contribution statement

Chiara Olla: Writing – original draft, Visualization, Methodology, Investigation, Formal analysis, Data curation, Conceptualization. **Alberto Martis:** Investigation, Data curation. **Carlo Barontini:** Investigation, Data curation. **Carlo Maria Carbonaro:** Writing – review & editing, Investigation, Formal analysis, Data curation. **Ignazio Roppolo:** Writing – review & editing, Investigation, Data curation. **Pier Carlo Ricci:** Writing – review & editing, Supervision. **Francesco Secci:** Writing – review & editing, Supervision. **Annalisa Chiappone:** Writing – review & editing, Supervision, Project administration, Funding acquisition.

Declaration of competing interest

The authors declare that they have no known competing financial interests or personal relationships that could have appeared to influence the work reported in this paper.

Acknowledgments

The authors gratefully acknowledge Livegreen Società Agricola Srl (Italy) for providing the biomass used in this study and Prof. Hansjörg Grützmacher (ETH, Zurich) for kindly supplying the BAPO-OH photoinitiator employed in this work. The authors also thank M. Marceddu and S. Lampis of the CeSAR (Centro Servizi Ricerca di Ateneo) core facility at the University of Cagliari for support with the ultrafast TR-PL/TA and NMR measurements. The authors thank M. Uccheddu and C. Mosino for their assistance with the experimental work. C.O. and C.M.C. acknowledge the COSY COST Action CA21101, funded by COST (European Cooperation in Science and Technology). C.O. and A.C. acknowledge funding from the European Union - Next Generation EU (PNRR), component M4C2, investment 1.1, PRIN 2022 PNRR Project "3D VOCe" (code P2022JWF3P), and from Fondazione di Sardegna, Italy through the FdS2022 F73C23002170007 Project "3D printed optical VOC sensors for indoor air quality evaluation".

Appendix A. Supplementary data

Supplementary material related to this article can be found online at https://doi.org/10.1016/j.susmat.2026.e02096.

Data availability

Data will be made available on request.

References

[1] R. Croce, H.V. Amerongen, Natural strategies for photosynthetic light harvesting, 2014, http://dx.doi.org/10.1038/nchembio.1555.
[2] R. Fernandes, J. Campos, M. Serra, J. Fidalgo, H. Almeida, A. Casas, D. Toubarro, A.I. Barros, Exploring the benefits of phycocyanin: From spirulina cultivation to its widespread applications, 2023, http://dx.doi.org/10.3390/ph16040592.
[3] B. Fernández-Rojas, J. Hernández-Juárez, J. Pedraza-Chaverri, Nutraceutical properties of phycocyanin, 2014, http://dx.doi.org/10.1016/j.jff.2014.10.011.
[4] A.H. Squires, W.E. Moerner, Direct single-molecule measurements of phycocyanobilin photophysics in monomeric C-phycocyanin, Proc. Natl. Acad. Sci. USA 114 (2017) 9779–9784, http://dx.doi.org/10.1073/pnas.1705435114.
[5] Y. Li, R. Gillilan, A. Abbaspourrad, Tuning C-phycocyanin photoactivity via pH-mediated assembly-disassembly, Biomacromolecules 22 (2021) 5128–5138, http://dx.doi.org/10.1021/acs.biomac.1c01095.
[6] Y. Li, Q. Li, R.E. Gillilan, A. Abbaspourrad, Reversible disassembly-reassembly of C-phycocyanin in pressurization-depressurization cycles of high hydrostatic pressure, Int. J. Biiol. Macromol. 253 (2023) http://dx.doi.org/10.1016/j.ijbiomac.2023.127623.
[7] E.Y. Parshina, W. Liu, A.I. Yusipovich, D.A. Gvozdev, Y. He, S.K. Pirutin, E.A. Klimanova, E.G. Maksimov, G.V. Maksimov, Spectral and conformational characteristics of phycocyanin associated with changes of medium pH, Photosynth. Res. 161 (2024) 93–103, http://dx.doi.org/10.1007/s11120-023-01068-0.

[8] M.C. Roda-Serrat, K.V. Christensen, R.B. El-Houri, X. Fretté, L.P. Christensen, Fast cleavage of phycocyanobilin from phycocyanin for use in food colouring, Food Chem. 240 (2018) 655–661, http://dx.doi.org/10.1016/j.foodchem.2017.07.149.
[9] S. Xiao, Z. Lu, J. Yang, X. Shi, Y. Zheng, Phycocyanobilin from arthrospira platensis: A potential photodynamic anticancer agent, Dye. Pigment. 219 (2023) http://dx.doi.org/10.1016/j.dyepig.2023.111516.
[10] Z. Ye, J. Fang, B. Yao, G. Liu, Heterologous expression of phycocyanobilin in escherichia coli and determination of its antioxidant capacity in vitro, Mol. Biotechnol. 67 (2025) 983–995, http://dx.doi.org/10.1007/s12033-024-01098-6.
[11] T. Watermann, H. Elgabarty, D. Sebastiani, Phycocyanobilin in solution-a solvent triggered molecular switch, Phys. Chem. Chem. Phys. 16 (2014) 6146–6152, http://dx.doi.org/10.1039/c3cp54307b.
[12] M. Bischoff, G. Hermann, S. Rentsch, D. Strehlow, S. Winter, H. Chosrowjan, Excited-state processes in phycocyanobilin studied by femtosecond spectroscopy, J. Phys. Chem. B 104 (2000) 1810–1816, http://dx.doi.org/10.1021/jp992083f.
[13] M. Theiß, M. Grupe, T. Lamparter, M.A. Mroginski, R. Diller, Ultrafast proton release reaction and primary photochemistry of phycocyanobilin in solution observed with fs-time-resolved mid-IR and UV/Vis spectroscopy, Photochem. Photobiol. Sci. 20 (2021) 715–732, http://dx.doi.org/10.1007/s43630-021-00045-7.
[14] B.J. Homoelle, W.F. Beck, Solvent Accessibility of the Phycocyanobilin Chromophore in the R Subunit of C-Phycocyanin: Implications for a Molecular Mechanism for Inertial Protein-Matrix Solvation Dynamics, Technical Report, 1995, URL https://pubs.acs.org/sharingguidelines.
[15] X. Sun, X. Liang, Y.K. Wang, P. Ma, W. Xiong, S. Qian, Y. Cui, H. Zhang, X. Chen, F. Tian, Y. Shi, F. Zheng, L. Li, A tumor microenvironment-activatable nanoplatform with phycocyanin-assisted in-situ nanoagent generation for synergistic treatment of colorectal cancer, Biomaterials 301 (2023) http://dx.doi.org/10.1016/j.biomaterials.2023.122263.
[16] H. Liang, Y. Sun, C. Li, H. Lin, Q. Huang, C. Li, Facile synthesis of phycocyanin/polydopamine hierarchical nanocomposites for synergizing PTT/PDT against cancer, RSC Adv. 12 (2022) 34815–34821, http://dx.doi.org/10.1039/d2ra05863d.
[17] S. Bharathiraja, H. Seo, P. Manivasagan, M.S. Moorthy, S. Park, J. Oh, In vitro photodynamic effect of phycocyanin against breast cancer cells, Molecules 21 (2016) http://dx.doi.org/10.3390/molecules21111470.
[18] S. Bharathiraja, P. Manivasagan, M.S. Moorthy, N.Q. Bui, B. Jang, T.T.V. Phan, W.K. Jung, Y.M. Kim, K.D. Lee, J. Oh, Photo-based PDT/PTT dual model killing and imaging of cancer cells using phycocyanin-polypyrrole nanoparticles, Eur. J. Pharmaceut. Biopharmaceut. 123 (2018) 20–30, http://dx.doi.org/10.1016/j.ejpb.2017.11.007.
[19] J. Dagnino-Leone, C.P. Figueroa, M.L. Castañeda, A.D. Youlton, A. Vallejos-Almirall, A. Agurto-Muñoz, J.P. Pérez, C. Agurto-Muñoz, Phycobiliproteins: Structural aspects, functional characteristics, and biotechnological perspectives, 2022, http://dx.doi.org/10.1016/j.csbj.2022.02.016.
[20] S. Morya, V.K. Chattu, W. Khalid, M.Z. Khalid, A. Siddeeg, Potential protein phycocyanin: an overview on its properties, extraction, and utilization, 2023, http://dx.doi.org/10.1080/10942912.2023.2271686.
[21] H. Chen, J. Deng, L. Li, Z. Liu, S. Sun, P. Xiong, Recent progress of natural and recombinant phycobiliproteins as fluorescent probes, 2023, http://dx.doi.org/10.3390/md21110572.
[22] A. Bavali, M. Afshar, A. Rahmatpanahi, Surface plasmon-enhanced fluorescence of spirulina microalgae via triangular silver nanoparticles, Spectrochim. Acta - Part A: Mol. Biomol. Spectrosc. 340 (2025) http://dx.doi.org/10.1016/j.saa.2025.126348.
[23] K. Bhayani, M. Mitra, T. Ghosh, S. Mishra, C-phycocyanin as a potential biosensor for heavy metals like Hg2+ in aquatic systems, RSC Adv. 6 (2016) 111599–111605, http://dx.doi.org/10.1039/c6ra22753h.
[24] A.S. Manna, S. Ghosh, T. Ghosh, N. Karchaudhuri, S. Das, A. Roy, D.K. Maiti, Smart luminescent materials for emerging sensors: Fundamentals and advances, Chem. – an Asian J. 20 (2025) http://dx.doi.org/10.1002/asia.202401328.
[25] H. Nawaz, S. Chen, X. Zhang, X. Li, T. You, J. Zhang, F. Xu, Cellulose-based fluorescent material for extreme pH sensing and smart printing applications, ACS Nano 17 (2023) 3996–4008, http://dx.doi.org/10.1021/acsnano.2c12846.
[26] W.K. Szapoczka, C. Olla, C. Carucci, A.L. Truskewycz, T. Skodvin, A. Salis, C.M. Carbonaro, B. Holst, P.J. Thomas, Ratiometric fluorescent pH sensing with carbon dots: Fluorescence mapping across pH levels for potential underwater applications, Nanomaterials 14 (2024) http://dx.doi.org/10.3390/nano14171434.
[27] A. Cocco, S. Paniziutti, C. Olla, R. Corpino, C.M. Carbonaro, P.C. Ricci, N. Melis, P. Caria, G. Sanna, E. Zysman-Colman, F. Secci, Design, synthesis, and photophysical characterization of biocompatible thermally activated delayed fluorescent carbazole-coumarins for sensing applications, Chem. Eur. J. 30 (2024) http://dx.doi.org/10.1002/chem.202401263.
[28] P. Enciso, F.M. Cabrerizo, J.S. Gancheff, P.A. Denis, M.F. Cerdá, Phycocyanin as potential natural dye for its use in photovoltaic cells, J. Appl. Solut. Chem. Model. 2 (2013) 225–233, http://dx.doi.org/10.6000/1929-5030.2013.02.04.3.
[29] Y. Zheng, Y. Ma, P. He, L. Yan, H. Cao, F. Shao, Phycocyanin/hyaluronic acid microneedle patches loaded with celastrol nanoparticles for synergistic treatment of diabetic nephropathy, ACS Biomater. Sci. Eng. 11 (2025) 371–382, http://dx.doi.org/10.1021/acsbiomaterials.4c01787.
[30] Z.P. Zhou, L.N. Liu, X.L. Chen, J.X. Wang, M. Chen, Y.Z. Zhang, B.C. Zhou, Factors that effect antioxidant activity of c-phycocyanins from spirulina platensis, 2005, http://dx.doi.org/10.1111/j.1745-4514.2005.00035.x.
[31] E.A. Lissi, M. Pizarro, A. Aspee, C. Romay, Original Contribution Kinetics of phycocyanine Bilin groups destruction by Peroxyl radicals, Technical Report, 2000.
[32] G. Feng, G. Wang, Q. Li, C. Han, D. Wei, J. Guo, Z. Wan, J. Wang, X. Yang, Depletion attraction driven formation of spirulina emulsion gels for 3D printing, Food Hydrocolloids 141 (2023) http://dx.doi.org/10.1016/j.foodhyd.2023.108691.
[33] S. Alotaiby, X. Zhao, C. Boesch, N.N. Sergeeva, Sustainable approach towards isolation of photosynthetic pigments from spirulina and the assessment of their prooxidant and antioxidant properties, Food Chem. 436 (2024) http://dx.doi.org/10.1016/j.foodchem.2023.137653.
[34] R. Lauceri, M. Bresciani, A. Lami, G. Morabito, Chlorophyll a interference in phycocyanin and allophycocyanin spectrophotometric quantification, 2018, http://dx.doi.org/10.4081/jlimnol.2017.1691.
[35] S. Marzorati, A. Schievano, A. Idà, L. Verotta, Carotenoids, chlorophylls and phycocyanin from spirulina: Supercritical CO2 and water extraction methods for added value products cascade, Green Chem. 22 (2020) 187–196, http://dx.doi.org/10.1039/c9gc03292d.
[36] A. Orona-Navar, I. Aguilar-Hernández, T. López-Luke, A. Pacheco, N. Ornelas-Soto, Dye sensitized solar cell (DSSC) by using a natural pigment from microalgae, Int. J. Chem. Eng. Appl. 11 (2020) 14–17, http://dx.doi.org/10.18178/ijcea.2020.11.1.772.
[37] M. Yusprianto, T.A. Zaharah, I.H. Silalahi, Bandgap energy of TiO2/M-Chlorophyll material (M=Cu2+, Fe3+), J. Kim. Sains Dan Apl. 24 (2021) 126–135, http://dx.doi.org/10.14710/jksa.24.4.126-135.
[38] R. Santonocito, A. Pappalardo, N. Tuccitto, A. Cavallaro, G.T. Sfrazzetto, Formaldehyde sensing by fluorescent organic sensors, 2025, http://dx.doi.org/10.1039/d5ob00858a.
[39] D. Kwak, Y. Lei, R. Maric, Ammonia gas sensors: A comprehensive review, 2019, http://dx.doi.org/10.1016/j.talanta.2019.06.034.
[40] G. Antonelli, A. Mencattini, M. Massimiani, V. Lacconi, J. Filippi, M. Losardo, M. D'Orazio, P. Casti, M. Bragaglia, G. Curci, F. Nanni, L. Campagnolo, E. Martinelli, Development of integrated optical biosensors based on low-cost stereolithography fabrication and multispectral signature for lab-on-chip applications, Sensors Actuators B: Chem. 401 (2024) http://dx.doi.org/10.1016/j.snb.2023.135009.
[41] A. Lambert, S. Valiulis, Q. Cheng, Advances in optical sensing and bioanalysis enabled by 3D printing, ACS Sensors 3 (2018) 2475–2491, http://dx.doi.org/10.1021/acssensors.8b01085.
[42] A. Camposeo, L. Persano, M. Farsari, D. Pisignano, Additive manufacturing: Applications and directions in photonics and optoelectronics, 2019, http://dx.doi.org/10.1002/adom.201800419.
[43] B. Tosetto, M. Gastaldi, G. Renno, C.F. Pirri, C. Barolo, A. Fin, I. Roppolo, Colorimetric 3D printable base-detectors exploiting halocromic core-substituted naphthalenediimides, Polym. Chem. 14 (2023) 1213–1223, http://dx.doi.org/10.1039/D2PY01593E.
[44] F. Frascella, G. González, P. Bosch, A. Angelini, A. Chiappone, M. Sangermano, C.F. Pirri, I. Roppolo, Three-dimensional printed photoluminescent polymeric waveguides, ACS Appl. Mater. & Interfaces 10 (2018) 39319–39326, http://dx.doi.org/10.1021/acsami.8b16036.
[45] G.C. Zittelli, G. Mugnai, M. Milia, B. Cicchi, A.S. Benavides, A. Angioni, P. Addis, G. Torzillo, Effects of blue, orange and white lights on growth, chlorophyll fluorescence, and phycocyanin production of arthrospira platensis cultures, Algal Res. 61 (2022) 102583, http://dx.doi.org/10.1016/j.algal.2021.102583.
[46] B. Thevarajah, S. Piyatilleke, P. Nimarshana, S. Koushalya, A. Malik, T.U. Ariyadasa, Exploring effective light spectral conversion techniques for enhanced production of spirulina-derived blue pigment protein, c-phycocyanin, Bioresour. Technol. 399 (2024) 130612, http://dx.doi.org/10.1016/j.biortech.2024.130612.
[47] A. Adjali, I. Clarot, Z. Chen, E. Marchioni, A. Boudier, Physicochemical degradation of phycocyanin and means to improve its stability: A short review, 2022, http://dx.doi.org/10.1016/j.jpha.2021.12.005.
[48] T. Wenzl, P. Robouch, A. Schaechtele, J. Haedrich, J. Stroka, Guidance Document on the Estimation of LOD and LOQ for Measurements in the Field of Contaminants in Feed and Food, Publications Office, 2016, p. 56.
[49] Y. Hou, M. Yan, Q. Wang, Y. Wang, Y. Xu, Y. Wang, H. Li, H. Wang, C-phycocyanin from spirulina maxima as a green fluorescent probe for the highly selective detection of mercury(II) in seafood, Food Anal. Methods 10 (2017) 1931–1939, http://dx.doi.org/10.1007/s12161-016-0759-0.
[50] Q. Chen, S. Li, H. Xiong, Q. Zhao, Effect of different extraction methods on physicochemical characteristics and antioxidant activity of C-phycocyanin from dry biomass of arthrospira platensis, Foods 11 (2022) http://dx.doi.org/10.3390/foods11091296.
[51] A. Walter, J.C. de Carvalho, V.T. Soccol, A.B.B. de Faria, V. Ghiggi, C.R. Soccol, Study of phycocyanin production from spirulina platensis under different light spectra, Braz. Arch. Biology Technol. 54 (2011) 675–682, http://dx.doi.org/10.1590/S1516-89132011000400005.
[52] R. Croce, G. Cinque, A.R. Holzwarth, R. Bassi, The Soret Absorption Properties of Carotenoids and Chlorophylls in Antenna Complexes of Higher Plants, Technical Report, 2000, pp. 221–231.

[53] M. Seibert, J.S. Connolly, Fluorescence properties of C-phycocyanin isolated from a thermophilic cyanobacterium, Photochem. Photobiol. 40 (1984) 267–271, http://dx.doi.org/10.1111/j.1751-1097.1984.tb04585.x.

[54] D. Guard-Friar, R. MacColl, D.S. Berns, B. Wittmershaus, R.S. Knox, Picosecond fluorescence of cryptomonad biliproteins. Effects of excitation intensity and the fluorescence decay times of phycocyanin 612, phycocyanin 645, and phycoerythrin 545, Biophys. J. 47 (1985) 787–793, http://dx.doi.org/10.1016/S0006-3495(85)83982-5.

[55] A. Holzwarth, J. Wendler, W. Wehrmeyer, Studies on chromophore coupling in isolated phycobiliproteins. i. picosecond fluorescence kinetics of energy transfer in phycocyanin 645 from chroomonas sp., Biochim. et Biophys. Acta (BBA) - Bioenerg. 724 (1983) 388–395, http://dx.doi.org/10.1016/0005-2728(83)90098-1.

[56] N.R. Murty, C.N. Cederstrand, E. Rabinowitch, Chlorophyll a fluorescence yield in live cells and solutions, Photochem. Photobiol. 4 (1965) 917–921, http://dx.doi.org/10.1111/j.1751-1097.1965.tb07940.x.

[57] Y. Shi, Y.J. Shiu, C. Su, S.H. Lin, K. li Han, Transient absorption of the chlorophyll a in ethanol, Chin. J. Chem. Phys. 19 (2006) 6–10, http://dx.doi.org/10.1360/cjcp2006.19(1).6.5.

[58] I.H.M. van Stokkum, M.G. Müller, A.R. Holzwarth, Energy transfer and radical-pair dynamics in photosystem I with different red chlorophyll a pigments, Int. J. Mol. Sci. 25 (2024) 4125, http://dx.doi.org/10.3390/ijms25074125.

[59] J. Aoki, T. Yarita, M. Hasegawa, M. Asayama, Development of a new extraction method and functional analysis of phycocyanobilin from unique filamentous cyanobacteria, J. Biotech. 395 (2024) 180–188, http://dx.doi.org/10.1016/j.jbiotec.2024.08.006.